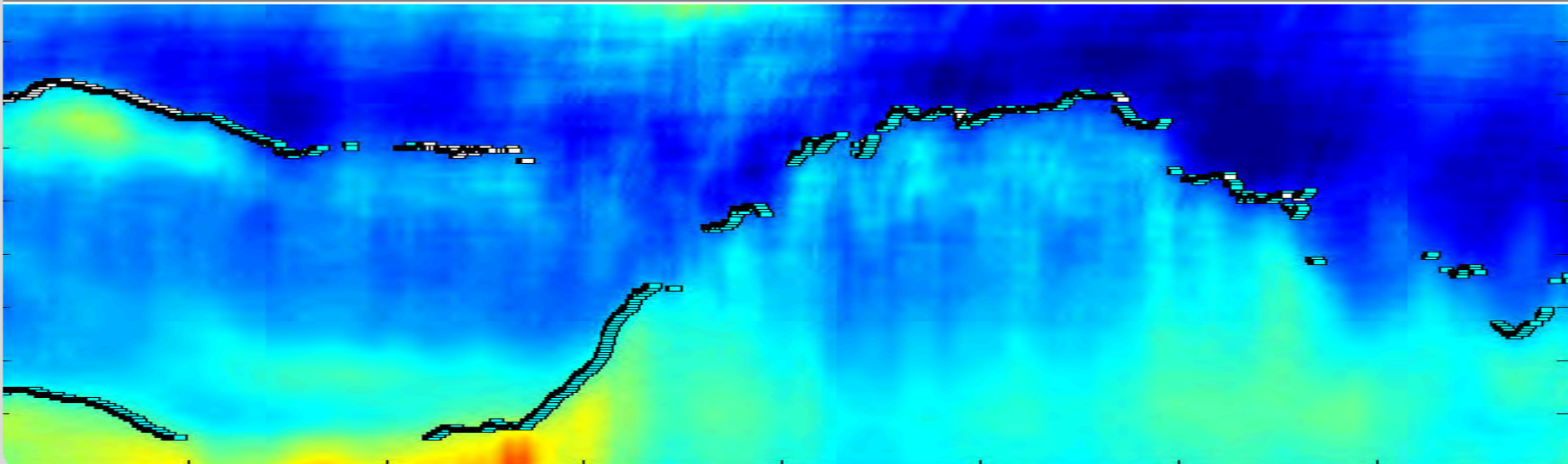


Remote sensing of mixing-layer height at environmental monitoring stations

Stefan Emeis
stefan.emeis@kit.edu

INSTITUTE OF METEOROLOGY AND CLIMATE RESEARCH, Atmospheric Environmental Research



Institute of Meteorology and Climate Research (IMK-IFU)

Atmospheric Environmental Research

Head: Prof. Dr. Hans Peter Schmid

Deputy Head: Prof. Dr. Hans Papen

Kst. 5260

Specialist Officer at
Establishment Level and
Safety Officer:

Sifa	E. Langer
Sibe	St. Schmid
SSB	Prof. Dr. H. Papen
Laser	Dr. T. Trickl

Bio-Geo-Chemical Processes

Head:
Prof. Dr. Klaus Butterbach-Bahl

Deputy Head: Prof. Dr. Hans Papen

Ecosystem-Atmosphere Interactions

Head: Prof. Dr. Almut Arneth

Regional Climate Systems

Head:
Prof. Dr. Harald Kunstmann

Deputy Head: Dr. Ralf Sussmann

Ecological Observatory TERENO-prealpine

Prof. Dr. Hans Papen

- Ecosystem Matter Fluxes
Dr. Ralf Kiese
- Regionalization of Biogenic Trace Gas Fluxes
Prof. Dr. Klaus Butterbach-Bahl

- Plant-Atmosphere Interactions
Prof. Dr. Almut Arneth
- Integrated Land-Atmosphere Surface-Exchange Research (iLASER)
Dr. Peter Werle
- Transport Processes in the Atmospheric Boundary-Layer (TABLE), Helmholtz-Young Investigators Group
Dr. Matthias Mauder

- Atmospheric Variability and Trends
Dr. Ralf Sussmann
- Regional Coupling of Ecosystem-Atmosphere-Processes
Dr. Peter Suppan
- Climate Change und Terrestrial Water Budget
Prof. Dr. Harald Kunstmann

World Calibration Center (WCC)

Dr. Rainer Steinbrecher

Helmholtz Research School MICMoR / Support of Young Scientists

Dr. B. Elija Bleher

Informationtechnology and Mechatronics

Head: Dipl.-Ing. Frank Neidl

Administration and Organization

Head: Prof. Dr. Hans Peter Schmid

TERENO

TERRESTRIAL ENVIRONMENTAL OBSERVATORIES

The Bavarian Prealpine Observatory

Hans Peter Schmid, Harald Kunstmann,
Hans Papen, Jean Charles Munch,
Eckart Priesack

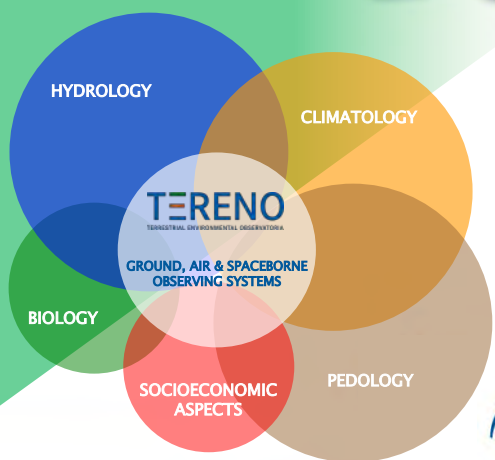
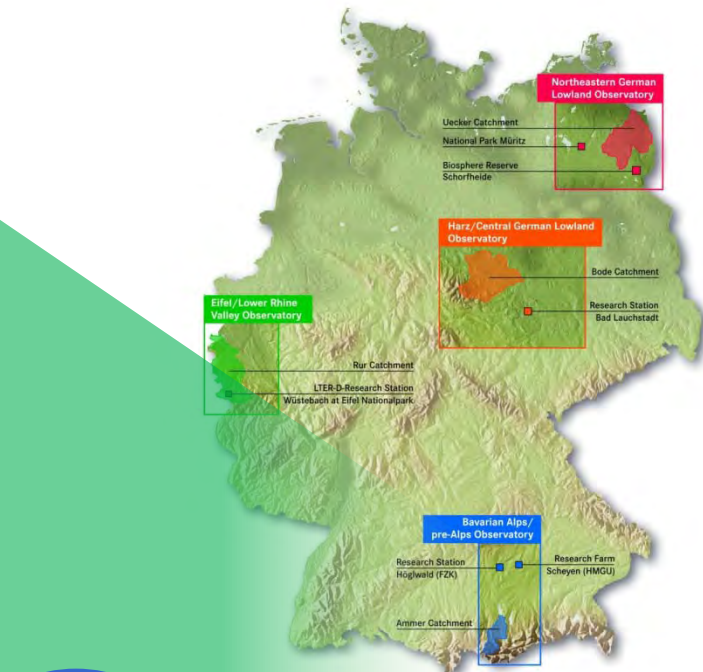
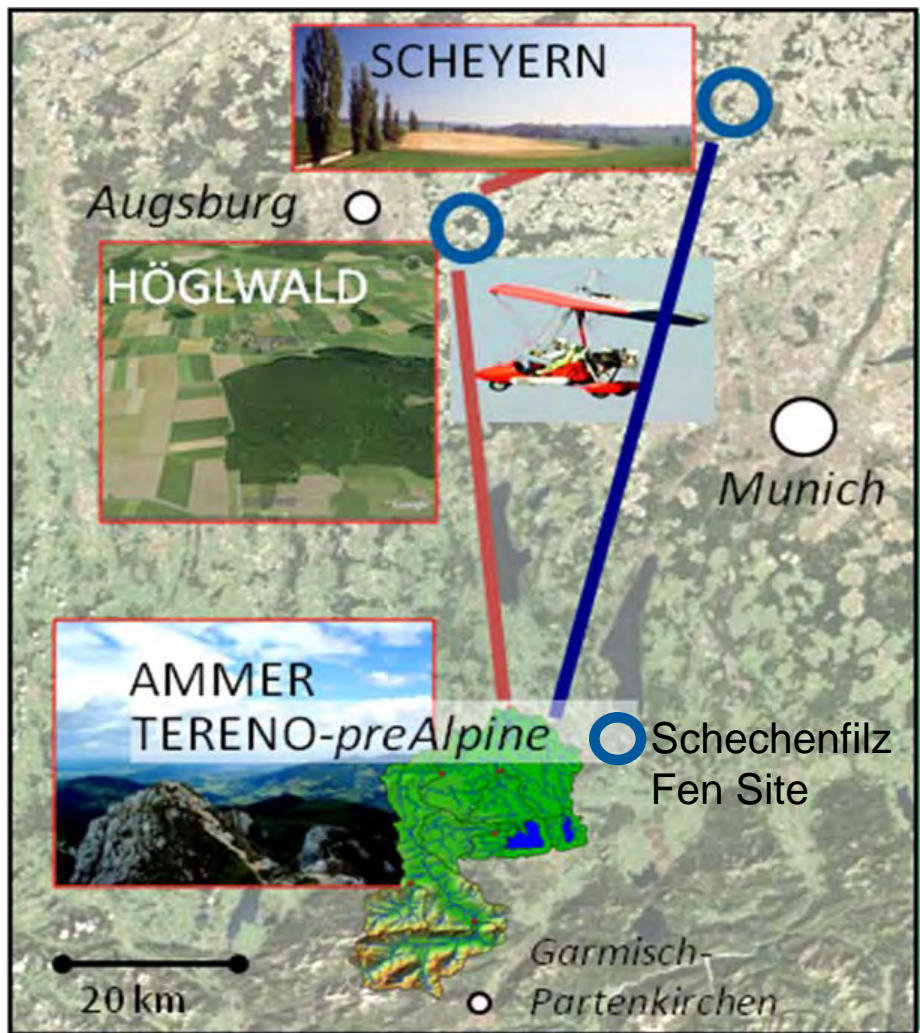




prealpine

TERENO
TERRESTRIAL ENVIRONMENTAL OBSERVATORIES

The Bavarian Prealpine Observatory



HELMHOLTZ
ASSOCIATION

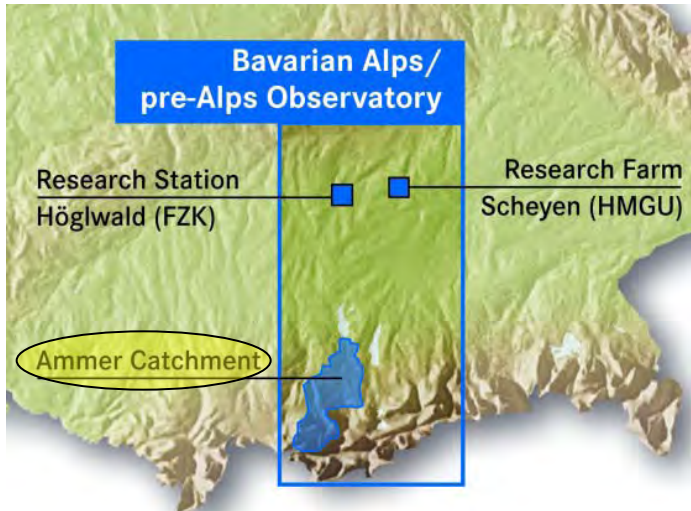


“In House” Research Goals

- Long-Term **biosphere-atmosphere exchange** (greenhouse gases, energy balance)
- Coupled **C/N-cycles** and C/N-storage
- **Vegetation and microbial biodiversity** (temporal dynamics, relation to matter turnover)
- **Alpine watershed hydrology** (water budget, Karst related problems, precipitation variability, floods/droughts, seepage water quality/quantity, water retention capacity)
- **Nutrient deposition** and **land use/management** (wet grasslands/fens, forests and agricultural systems).
- **Methodology development** for micrometeorological observations in complex terrain
- (planned) ecosystem-atmosphere exchange in **urban areas**



Ammer Catchment Observatory



- area of ~710 km² (601 km² above Weilheim)
- alpine and prealpine landscape with high spatial differentiation in geology and pedology
- elevations: from 533 m (a.s.l., Ammersee) to 2185 m (Kreuzspitze)
- two dominant landscape units: the prealpine hill country and moorland and the Swabian-Upper Bavarian foothills of the Alps.
- Dominant geology: lime-alpine zone (south), flysch zone (north)

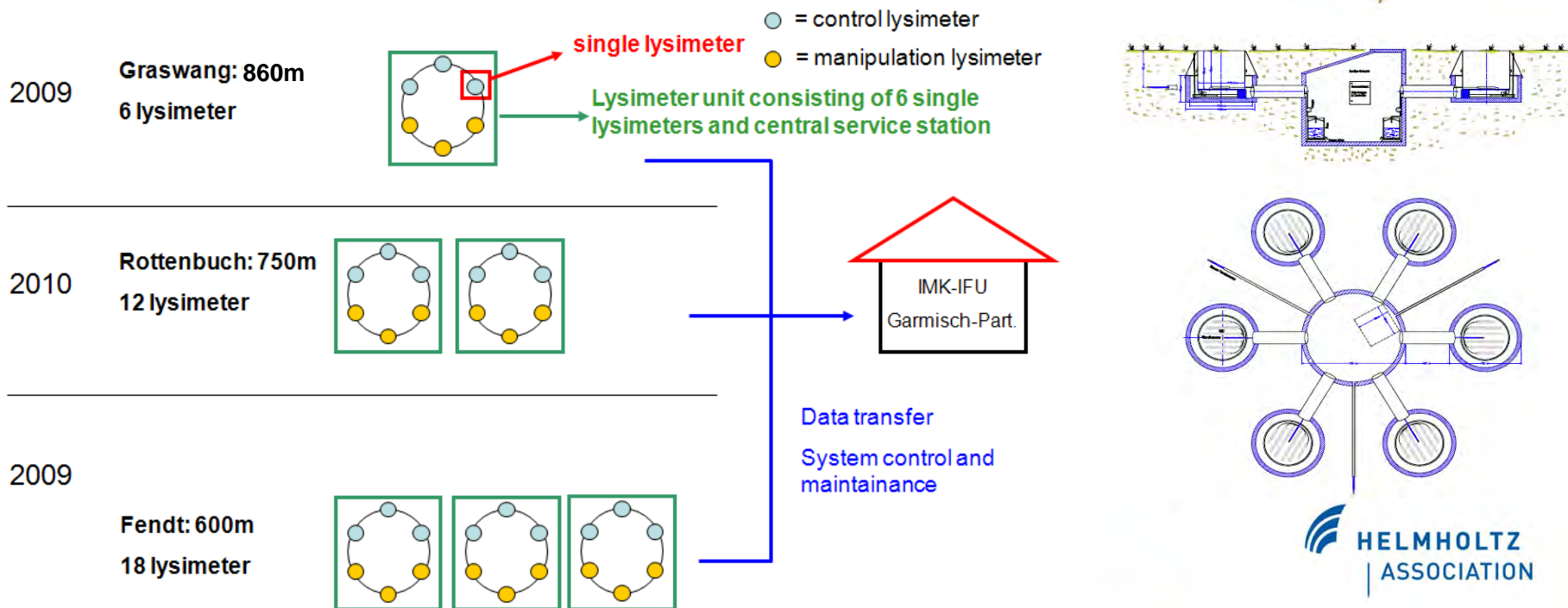
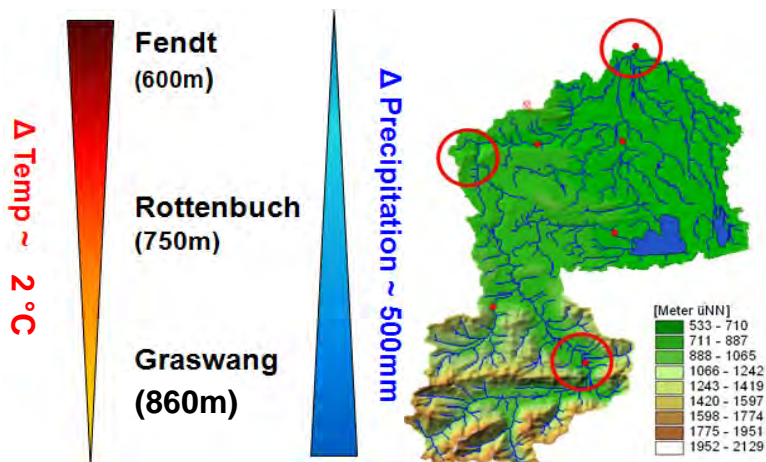
TERENO Infrastructure

- **Graswang-, Rottenbuch-, Fendt Sites**
 - 3 EC towers: momentum, heat, H₂O, CO₂, plus TERENO-ICOS: N₂O, CH₄ fluxes
 - 36 Lysimeters: soil water balance, **3 kilometers**
 - GHG (N₂O, CO₂, CH₄) measurements at lysimeters
- **Geigersau Site:** 1 X-Band precipitation radar
- **Sites to be determined:** 3 Climate stations
- **movable:** **1 Doppler wind lidar**



Climasequence: how do grassland ecosystems adapt to climate change?

- grassland soil monoliths transplanted along the natural gradient in temperature and precipitation
- climate change effects on C/N cycles
- associated plant and microbial processes/populations/biodiversity
- terrestrial hydrology and water quality





prealpine

TERENO
TERRESTRIAL ENVIRONMENTAL OBSERVATORIES

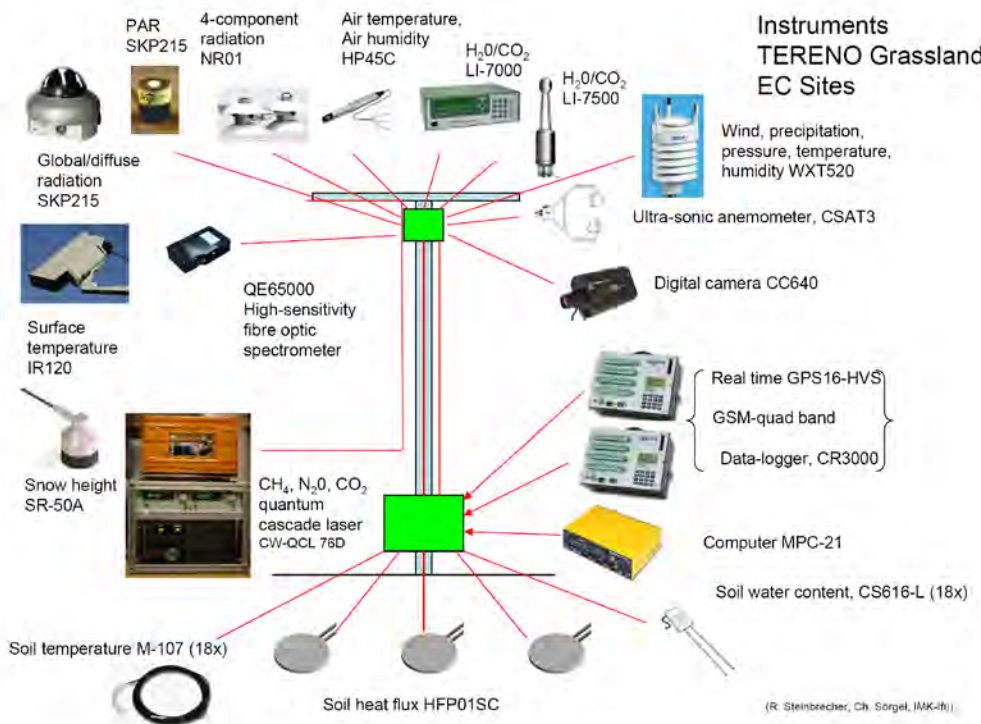
TERENO Lysimeter experiment: construction phase



 HELMHOLTZ
ASSOCIATION

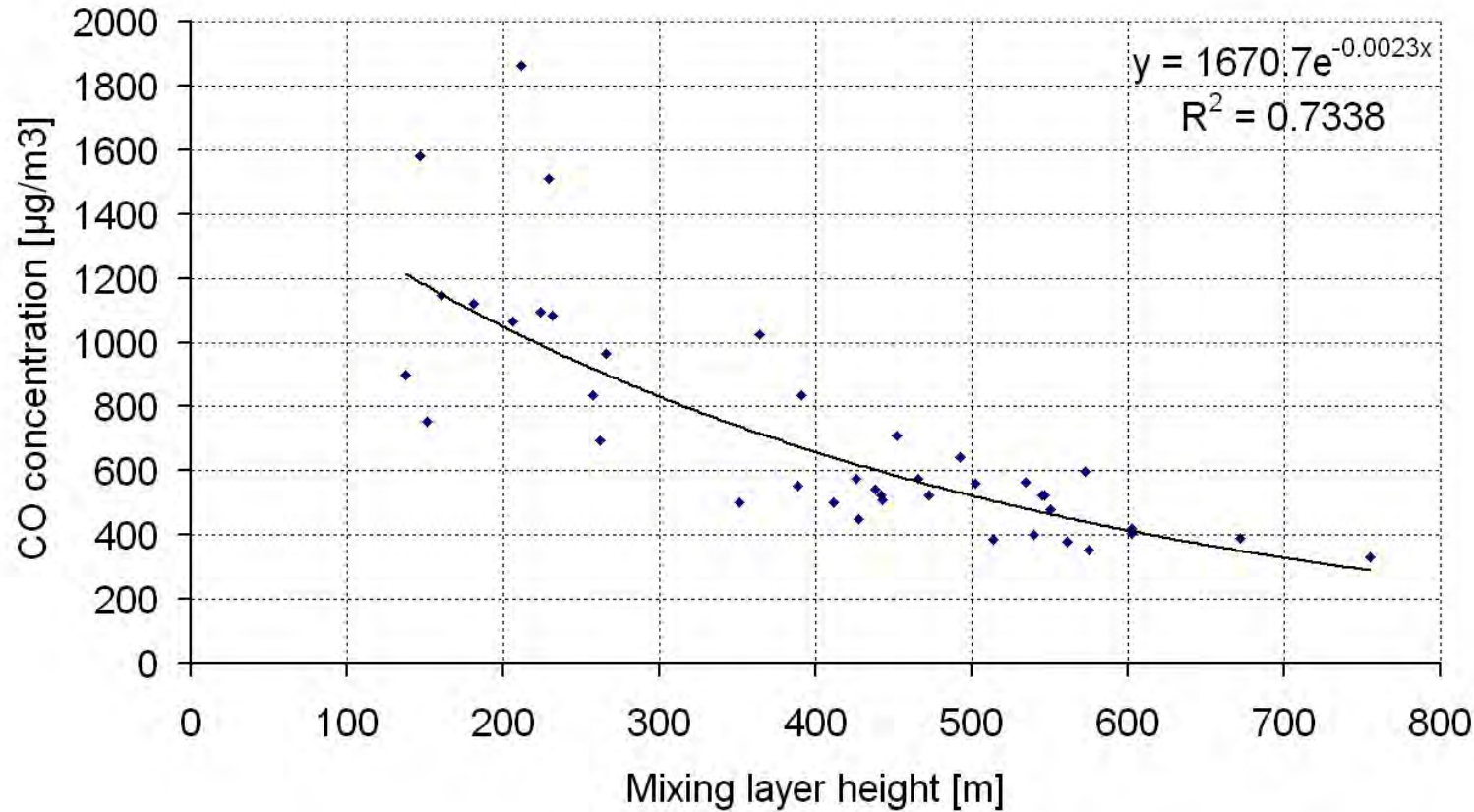


- ICOS mission: “To provide the long-term observations required to understand the present state and predict future behavior of the global carbon cycle and greenhouse gas emissions.”
- 5 EC-sites at TERENO-prealpine, -Harz, and –Eifel received additional funding to expand instrumentation to include fluxes of CH₄ and N₂O and upgrade to ICOS standard



Motivation

correlation at street level pollutant - MLH



Schäfer, K., S. Emeis, H. Hoffmann, C. Jahn, 2006: Influence of mixing layer height upon air pollution in urban and sub-urban areas. Meteorol. Z., 15, 647-658.

Remote sensing

of the vertical structure of the atmospheric boundary layer

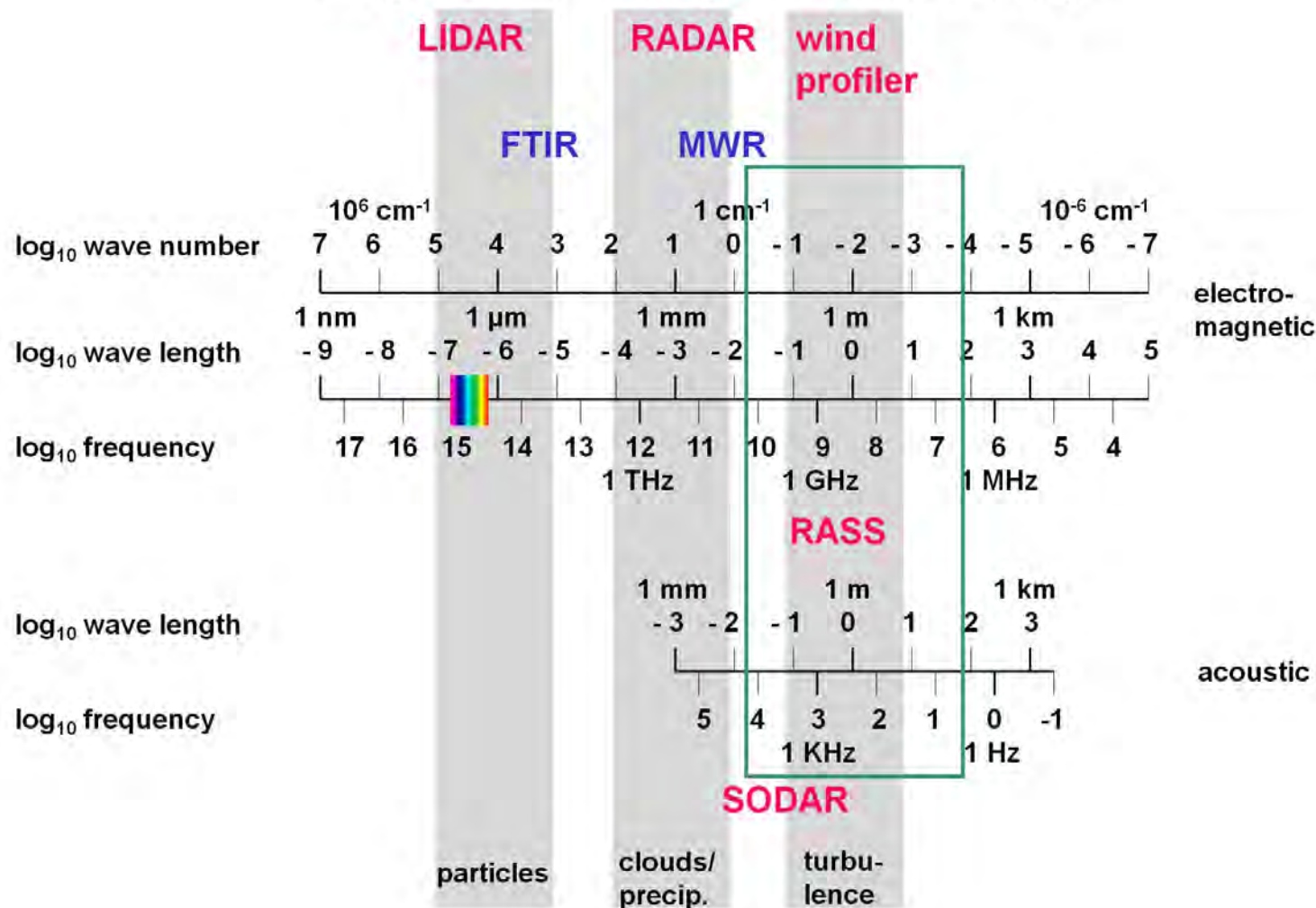
Basic remote sensing techniques

subject of this lecture

subject of this lecture

name	principle	spatial resolution	direction	type
RADAR	backscatter, electro-magnetic pulses, fixed profiling wave length		scanning, slanted	active, monostatic
SODAR	backscatter, acoustic pulses, fixed wave length	profiling	fixed, slanted, vertical	active, usually monostatic
LIDAR ceilometer	backscatter, optical pulses, fixed wave length(s)	profiling	scanning, fixed, horizontal, slanted, vertical	active, monostatic
RASS	backscatter, acoustic, electro-magnetic, fixed wave length	profiling	fixed, vertical	active, monostatic
FTIR	absorption, infrared, spectrum	path-averaging	fixed, horizontal, slanted	active, bistatic or passive
	emission, infrared, spectrum	path-averaging	fixed, horizontal, slanted	passive
DOAS	absorption, optical, fixed wave lengths	path-averaging	fixed, horizontal	active, bistatic
radiometry	electro-magnetic, fixed wave length(s)	averaging, profiling	fixed, scanning, slanted, vertical	passive
tomography	travel time, acoustic, fixed wave length	horizontal distribution	fixed, horizontal	active, multiple emitters and receivers

Frequencies for atmospheric remote sensing



Emeis, S., 2010: Measurement Methods in Atmospheric Sciences - In situ and remote. Borntraeger, Stuttgart, 272 pp., 103 figs, 28 tables, ISBN 978-3-443-01066-9.

Surface-based Remote Sensing Systems

at IMK-IFU

SODAR (Large system),
acoustic backscatter, Doppler
shift analysis → wind, turbulence



SODAR-RASS (Doppler-RASS), acoustic,
electro-magnetic backscatter, determines speed
of sound → wind and temperature profiles



Ceilometer,
backscatter, optical
pulses, wave
length ~ 0.9 µm
→ aerosol profiles



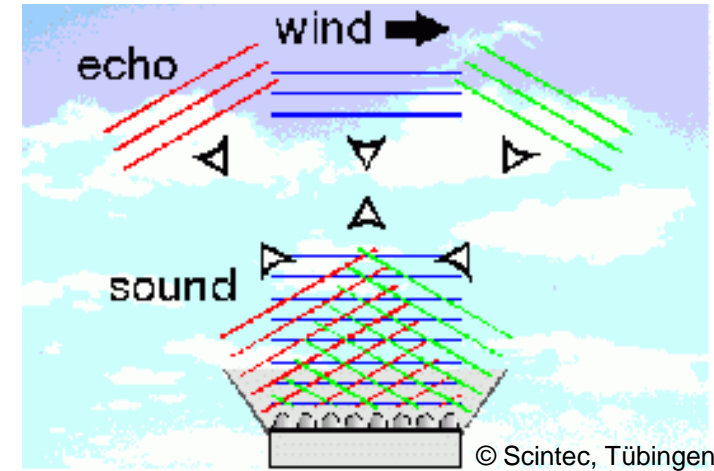
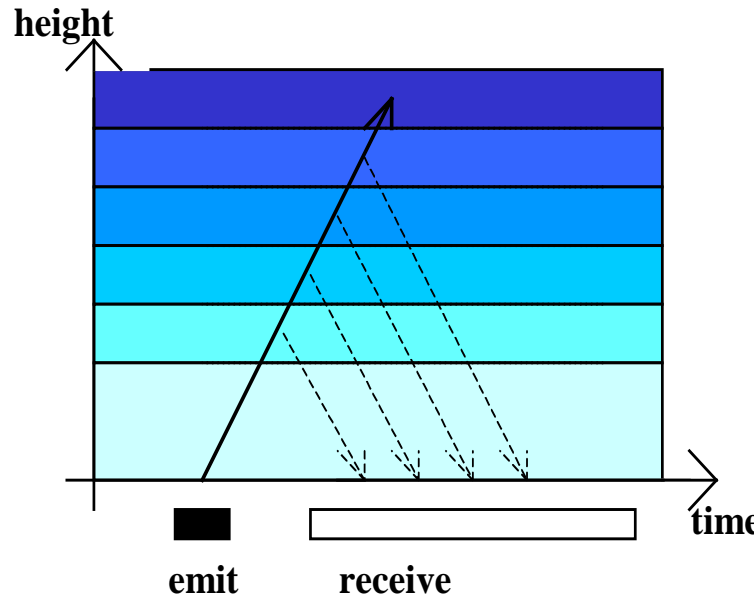
image:
Halo Photonics

SODAR

**algorithms for the determination of
mixing-layer height**

and low-level jet observations

monostatic SODAR: measuring principles



© Scintec, Tübingen

deduction:

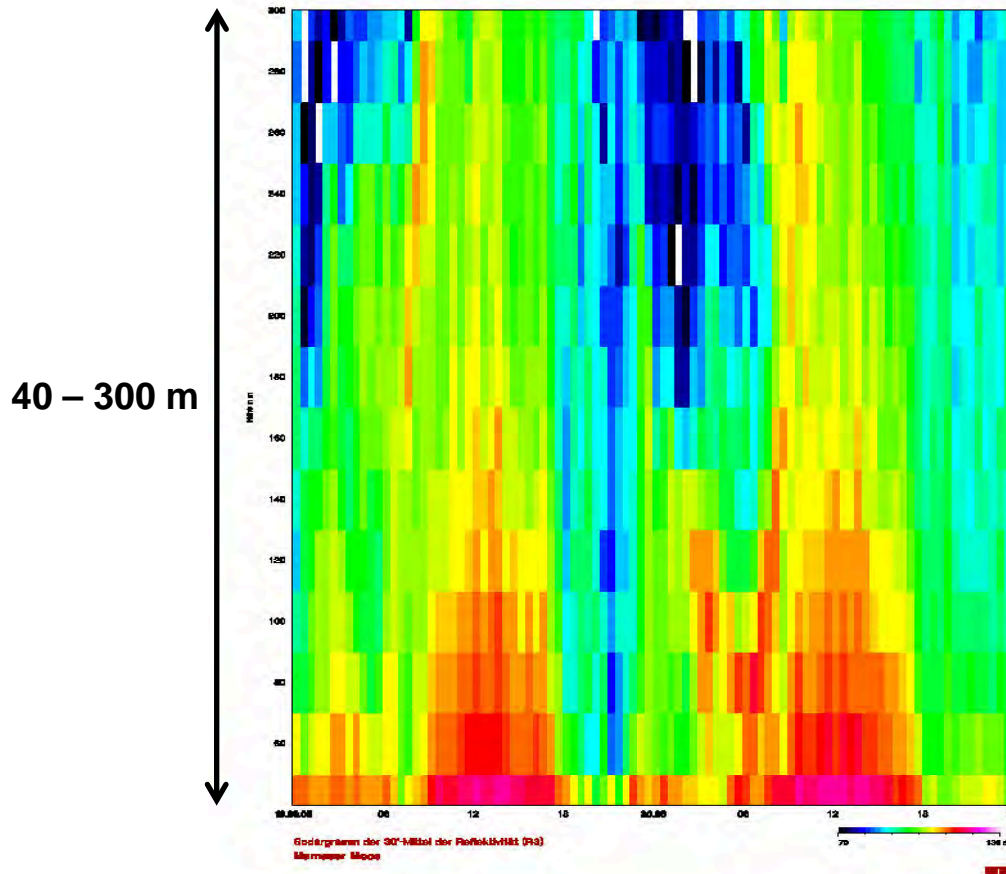
sound travel time	= height
backscatter intensity	= turbulence
Doppler-shift	= wind speed

Emission of sound waves
into three directions:

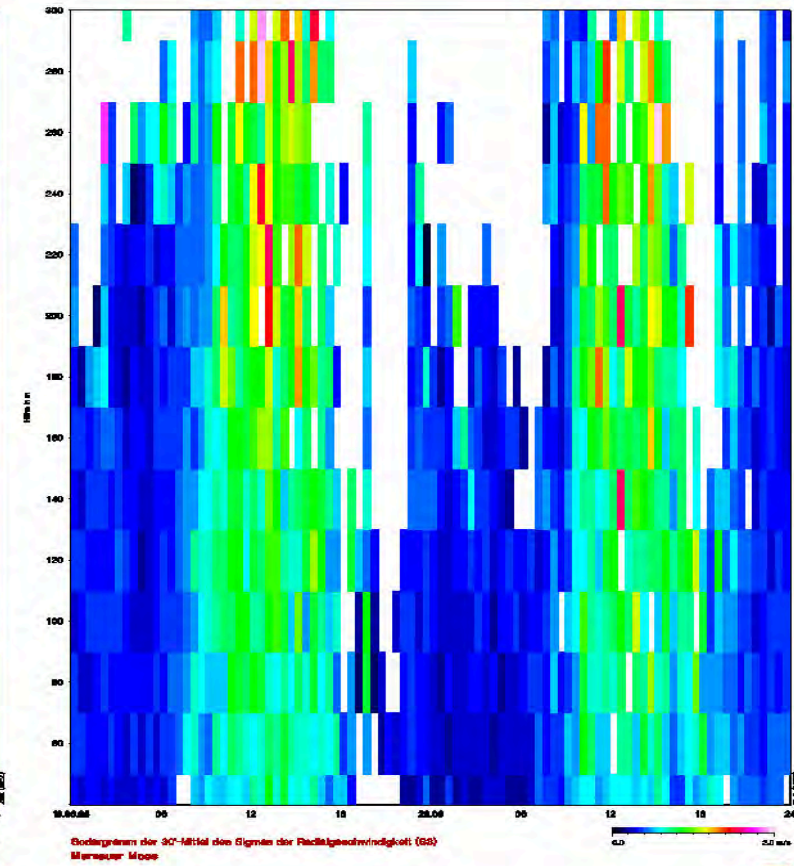
in order to measure all three
components of the wind
(horizontal and vertical)

SODAR sample plot (daytime convective BL)

acoustic backscatter intensity

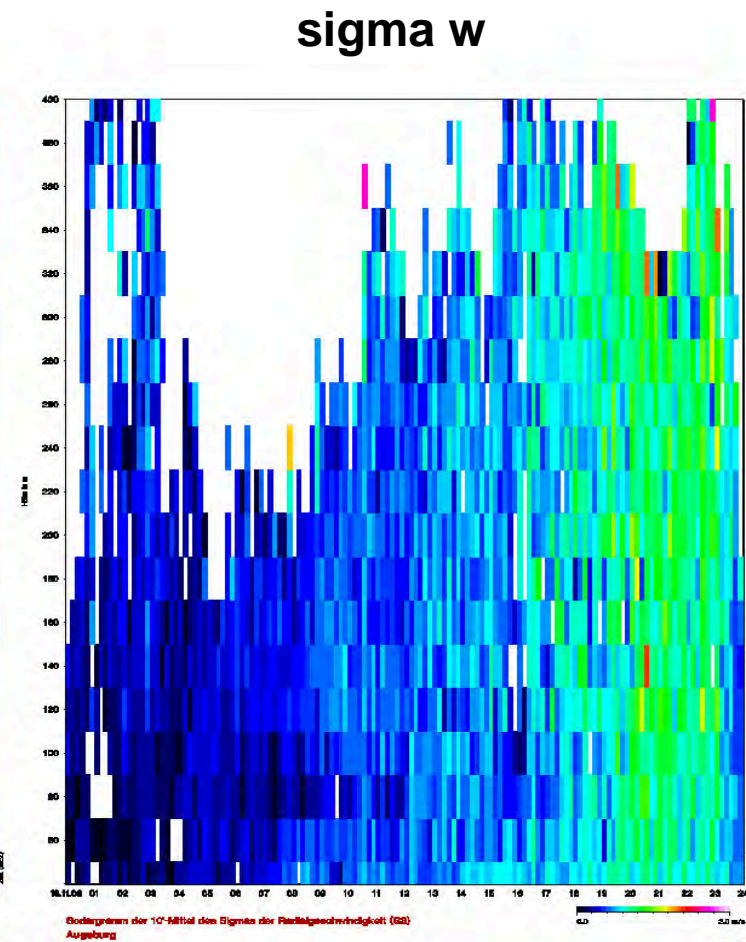
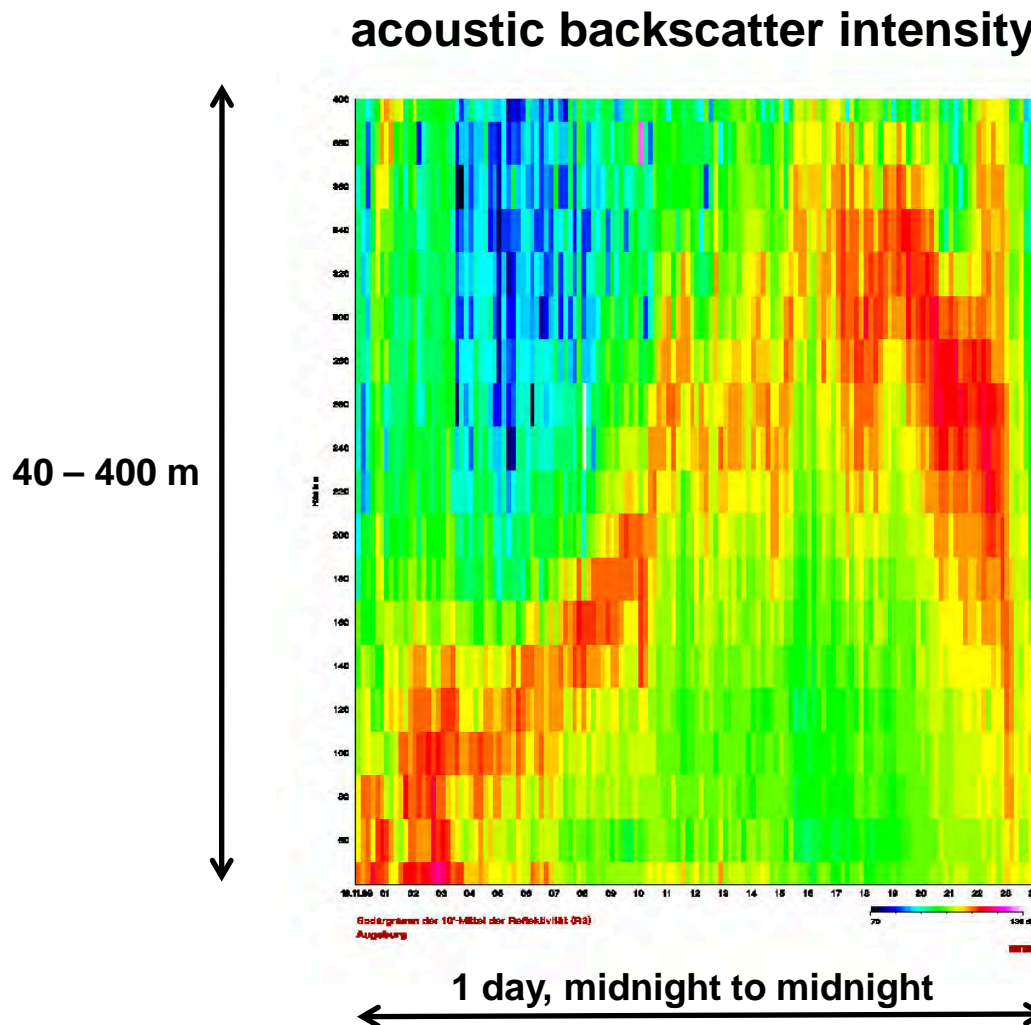


σ_w



2 days, midnight to midnight

SODAR sample plot (lifted inversion)



Algorithms to detect MLH from SODAR data

criterion 1:

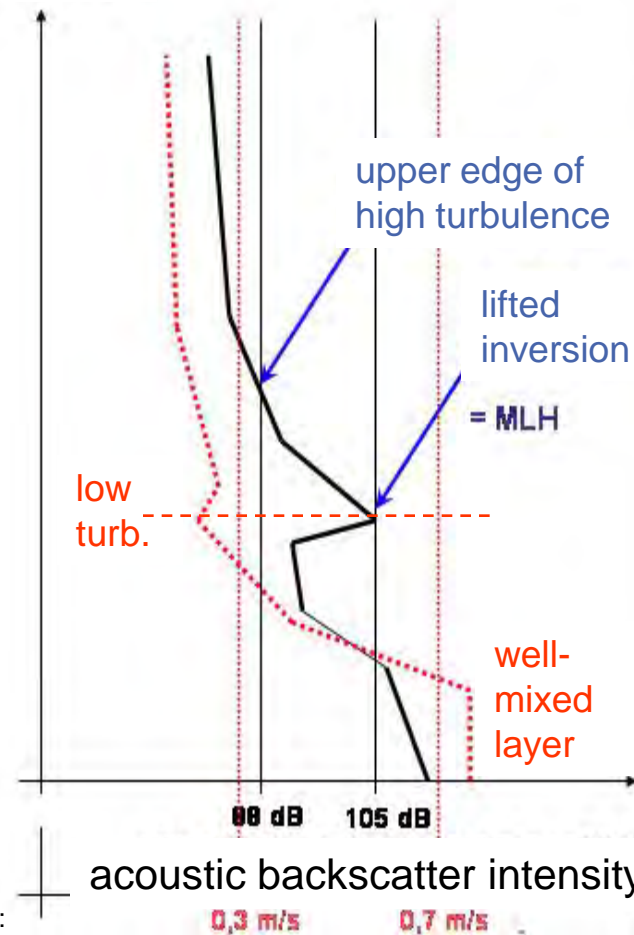
upper edge
of high
turbulence

criterion 2:

surface and
lifted
inversions

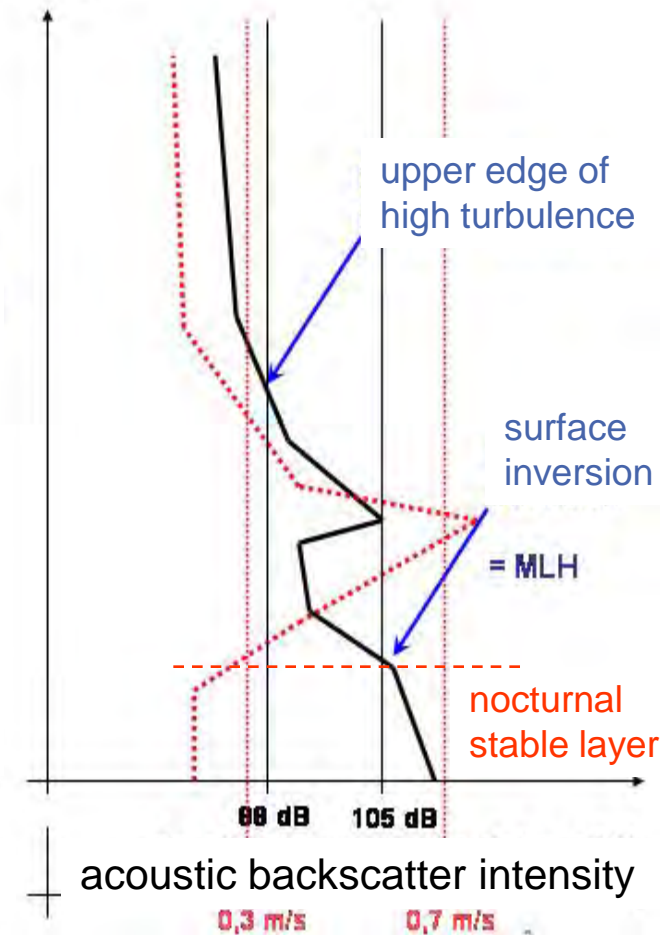
$$\text{MLH} = \text{Min} (\text{C1}, \text{C2})$$

height



example 1: daytime

height



example 2: night-time

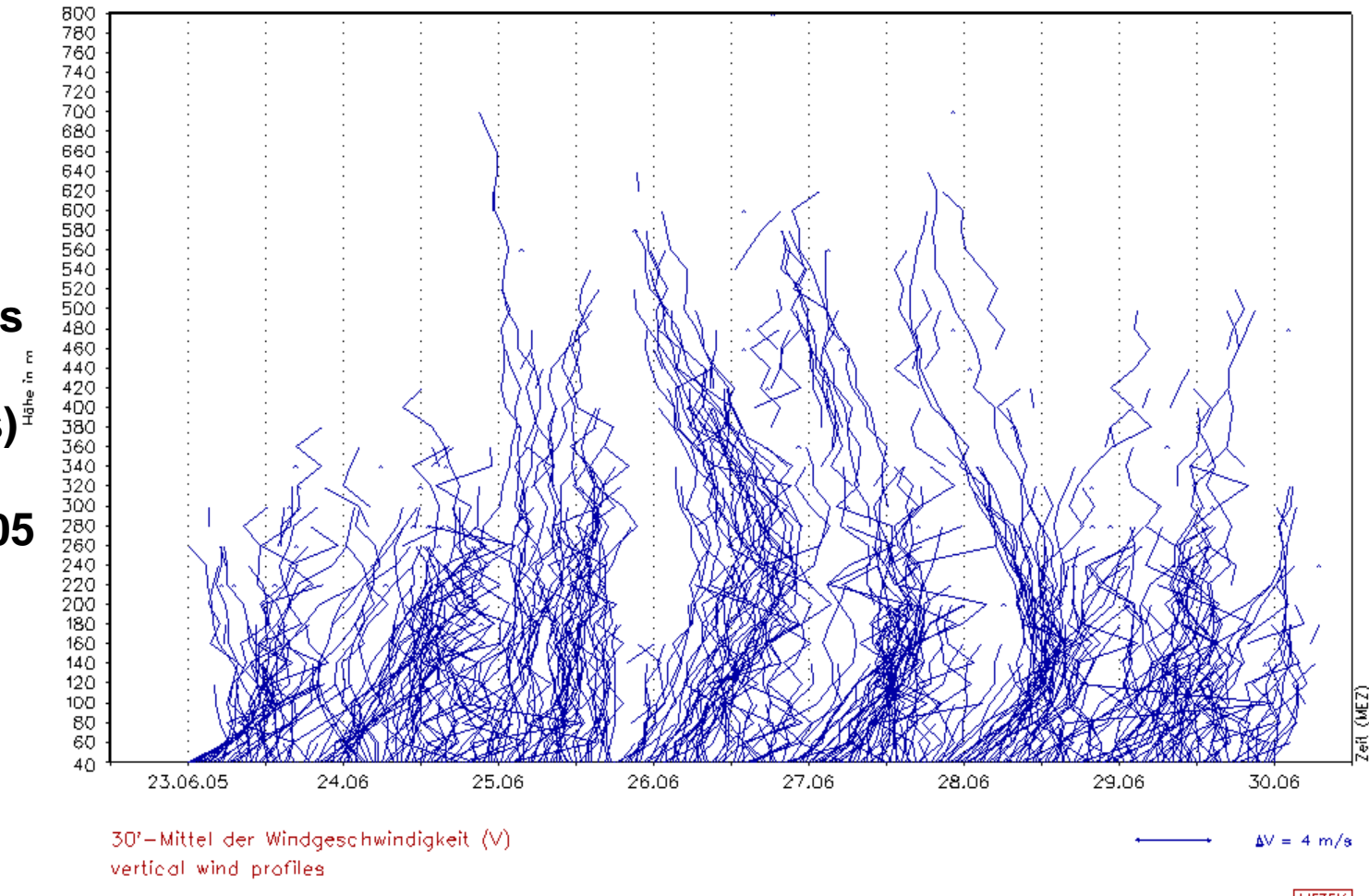
Emeis, S., K. Schäfer, C. Münkel, 2008:
Surface-based remote sensing of the
mixing-layer height – a review.

Meteorol. Z., 17, 621-630.

**vertical profiles
of wind speed
(30 min means)**

23-30 June 2005

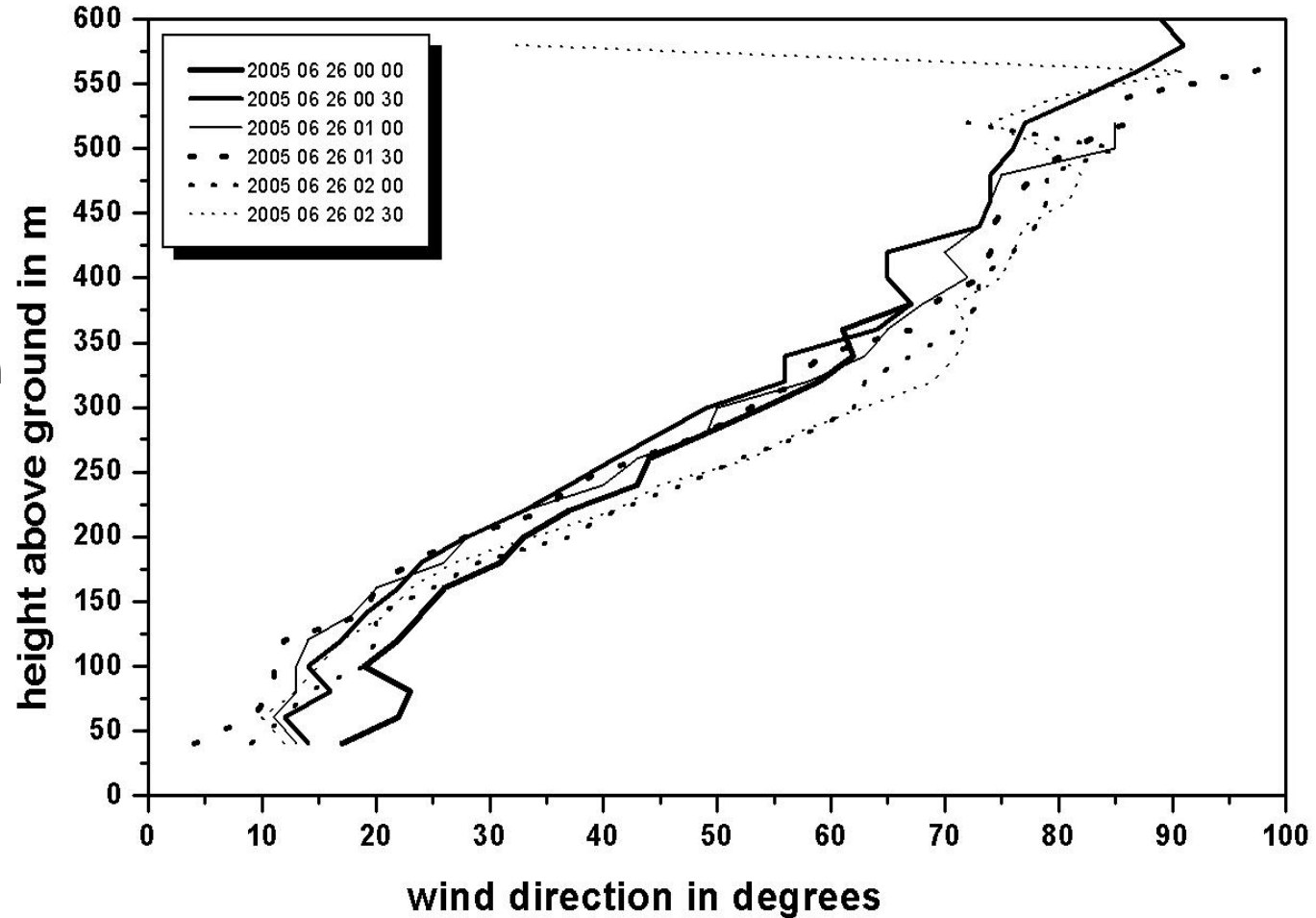
AdP Ch d G



vertical profiles
of wind direction

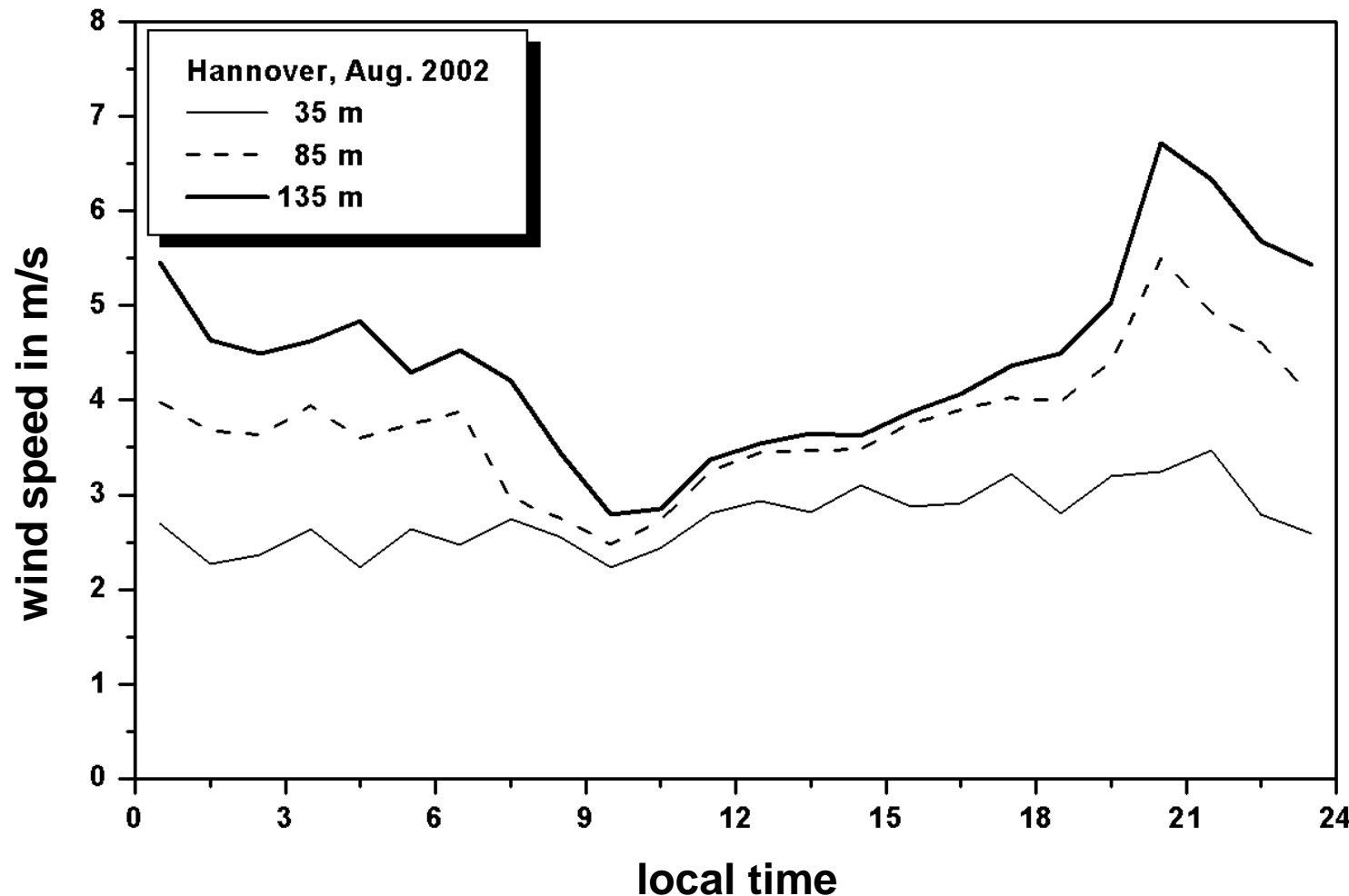
26 June 2005

AdP Ch d G

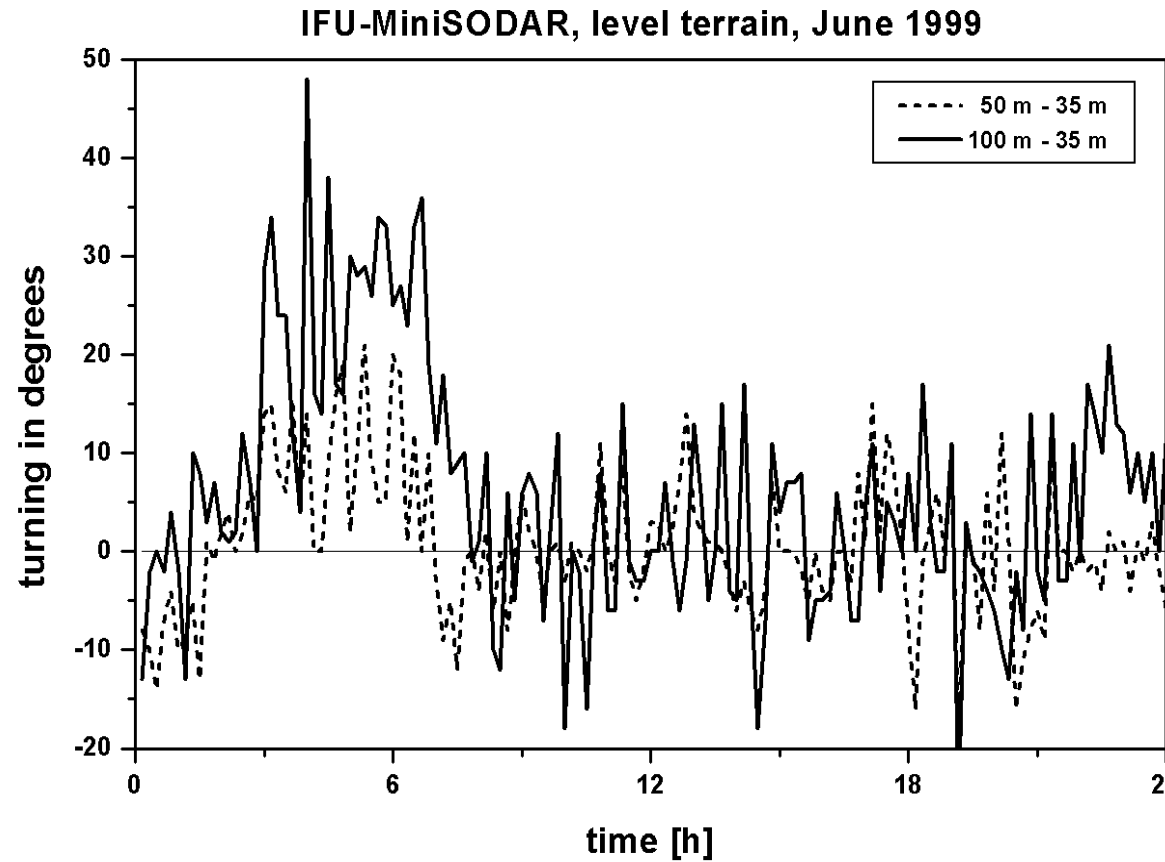


Monthly mean diurnal course of wind speed

August 2002, 17 nights with LLJ



Mean diurnal variation of the turning of wind direction with height

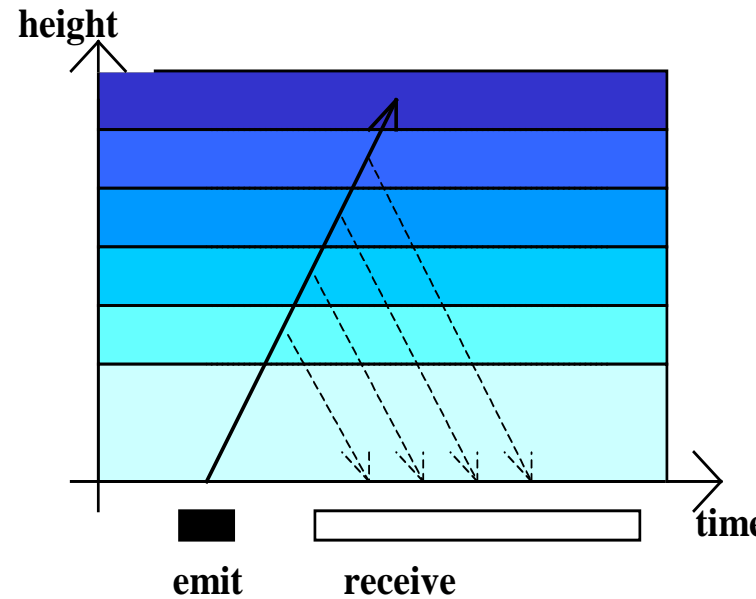


Emeis, S., 2001: Vertical variation of frequency distributions of wind speed in and above the surface layer observed by sodar. Meteorol. Z., **10**, 141-149.

Ceilometer

**algorithms for the determination of
mixing-layer height**

Ceilometer/LIDAR measuring principle

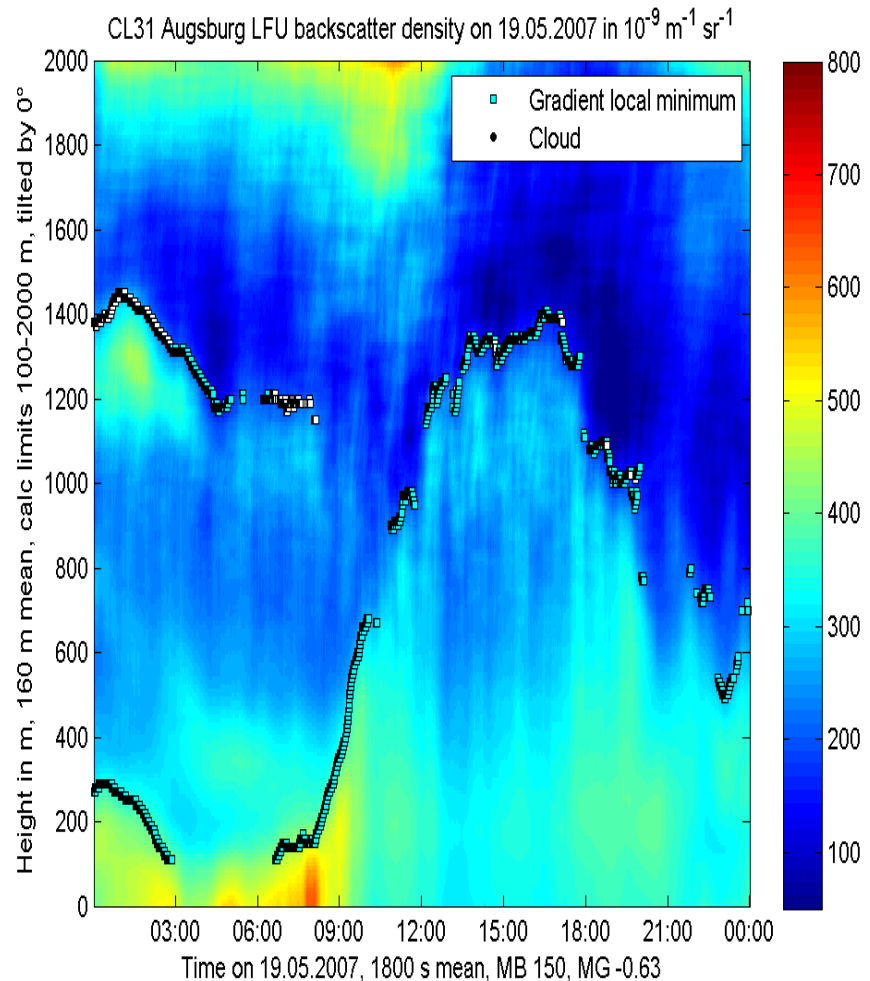


detection:

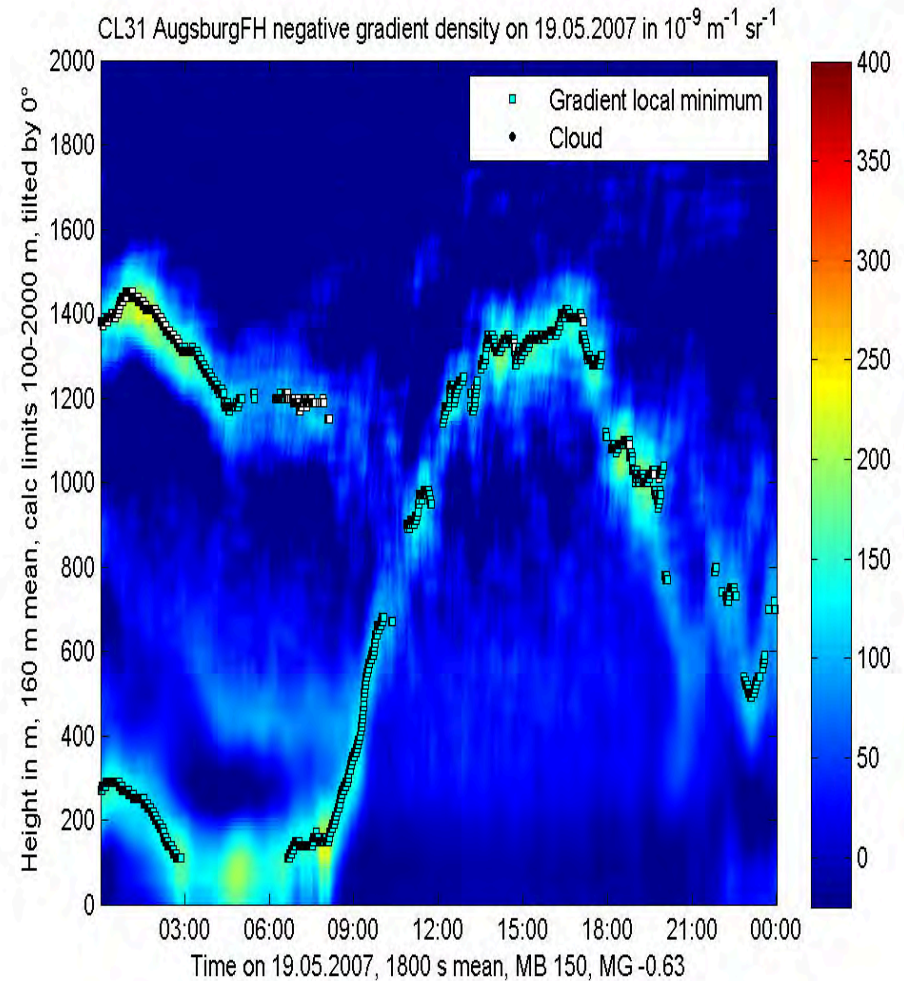
- | | |
|---|---|
| travel time of signal
backscatter intensity
Doppler-shift | = height
= particle size and number distribution
= cannot be analyzed from ceilometer data
(available only from a Wind-LIDAR: velocity component in line of sight) |
|---|---|

ceilometer sample plot (daytime convective BL)

optical backscatter intensity



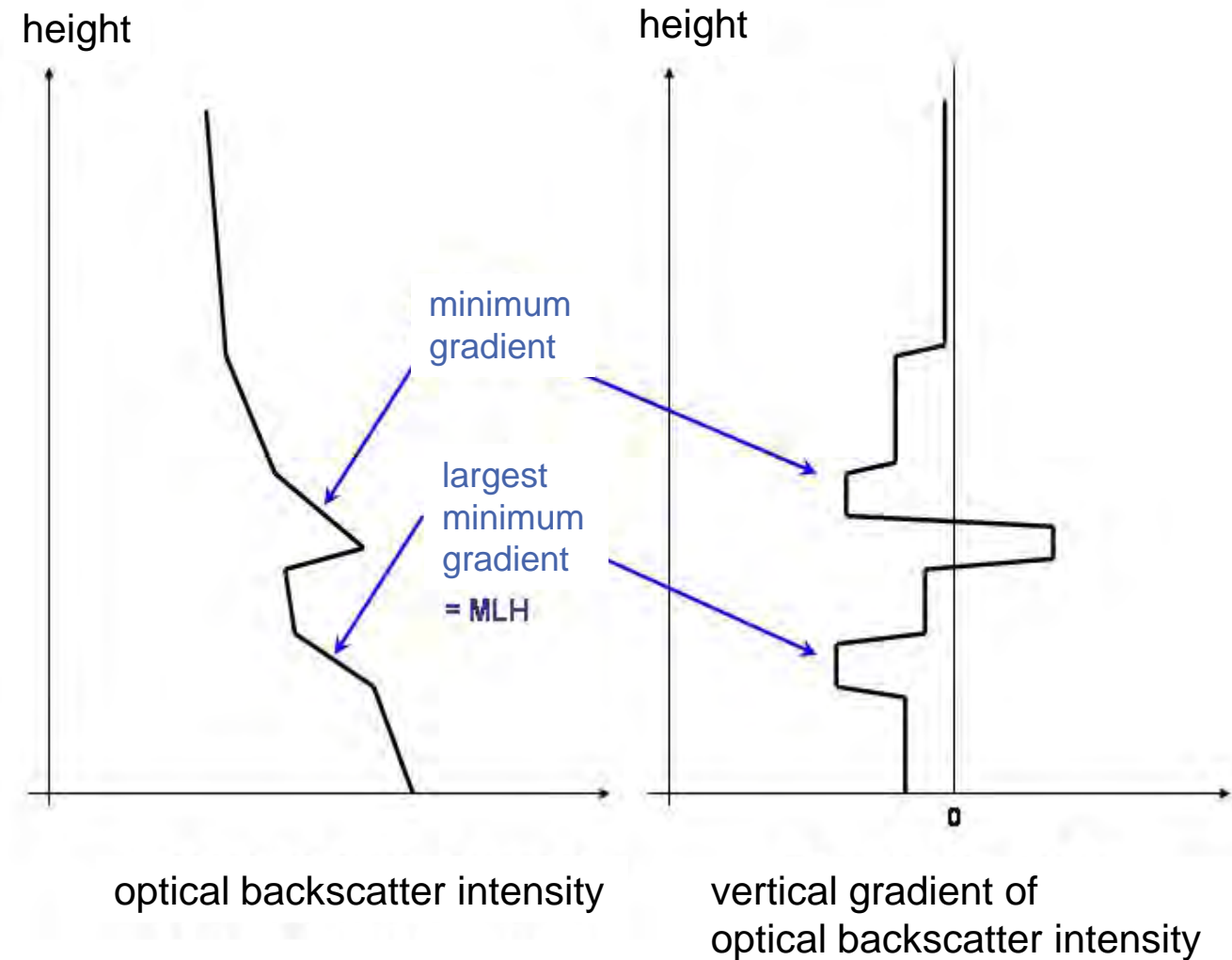
**negative vertical gradient of
optical backscatter intensity**



Algorithm to detect MLH from Ceilometer-Daten

criterion

minimal vertical
gradient of backscatter
intensity (the most
negative gradient)

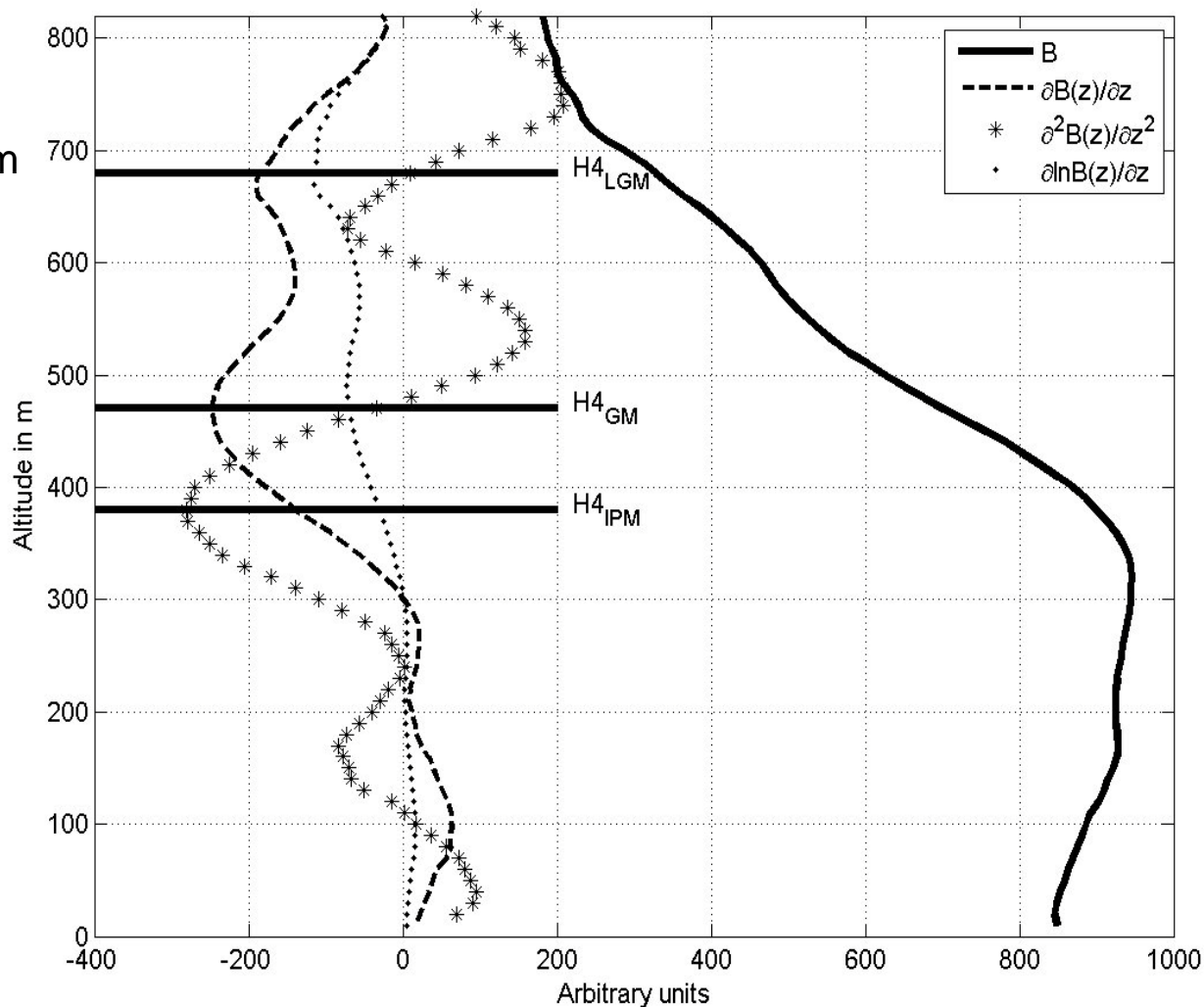


Different gradient methods (see Sicard et al. 2006, BLM 119, 135-157)

logarithmic gradient minimum

gradient minimum

inflection point method
(minimum of 2nd derivative)



comparison of two different ceilometers

LD40

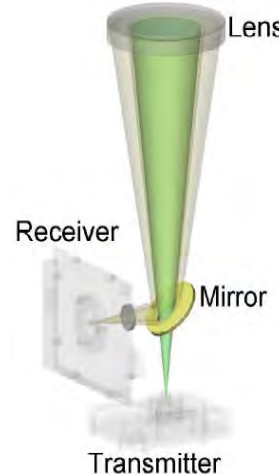
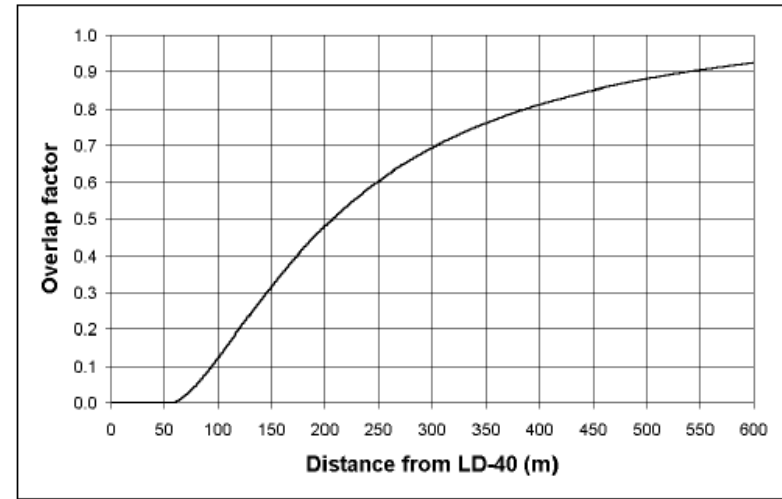
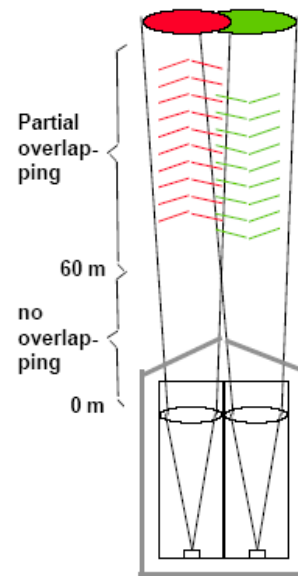
two optical axes

wave length: 855 nm
height resolution: 7.5 m
max. range: 13000 m

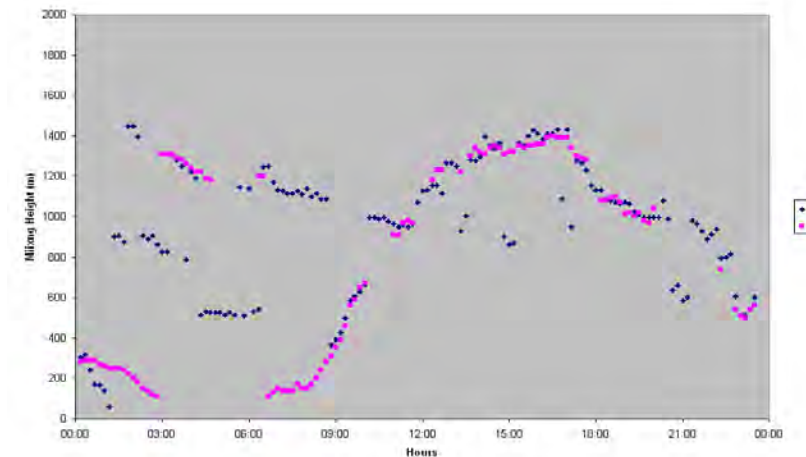
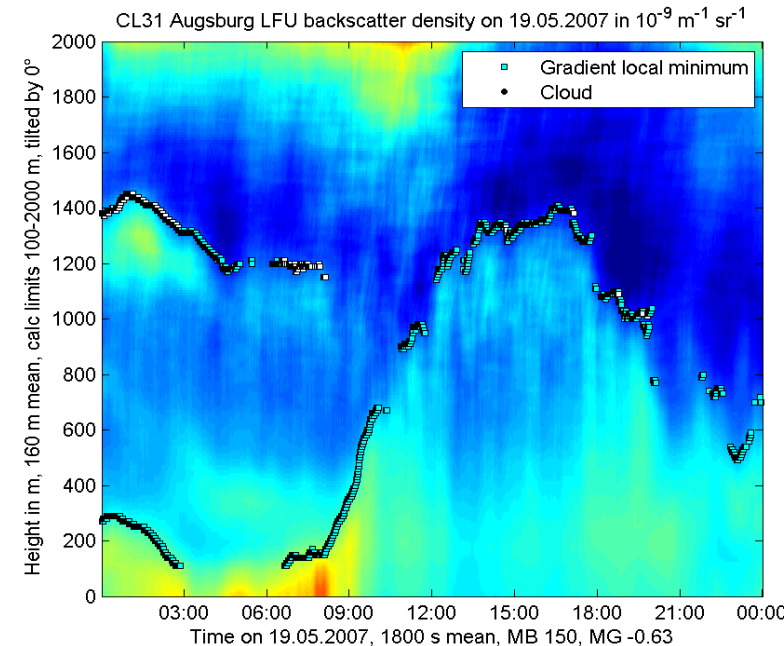
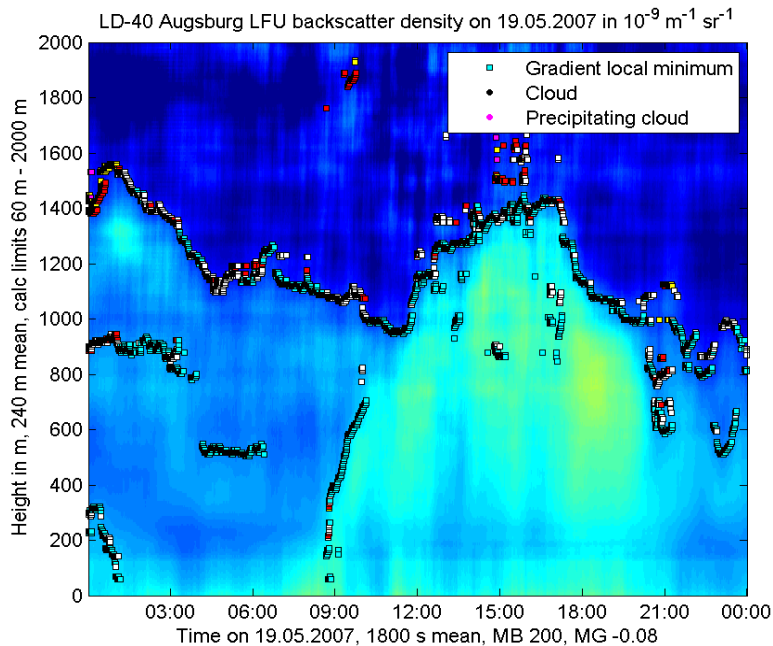
CL31 / CL51

one optical axis

wave length: 905 nm
height resolution: 5 m
max. range: 7500 m



comparison of LD40 and CL31

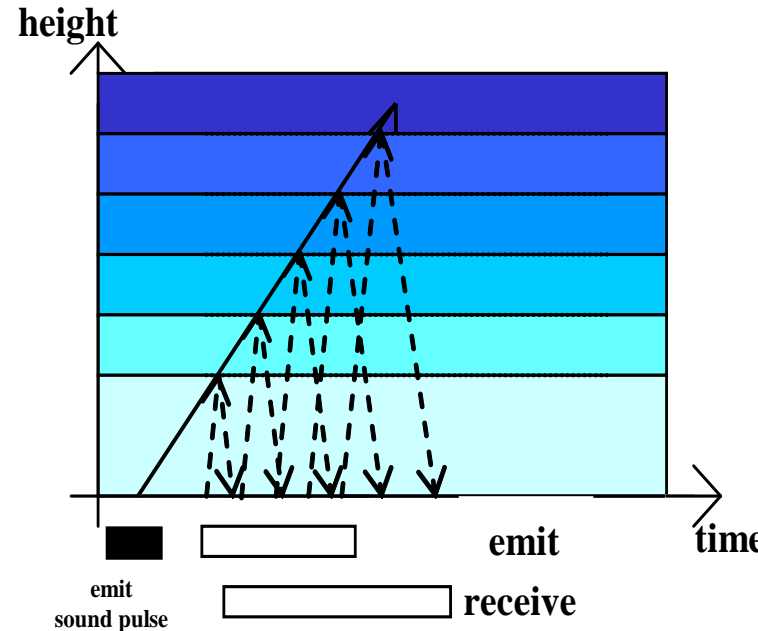


RASS

principles of operation

examples

RASS measuring principle



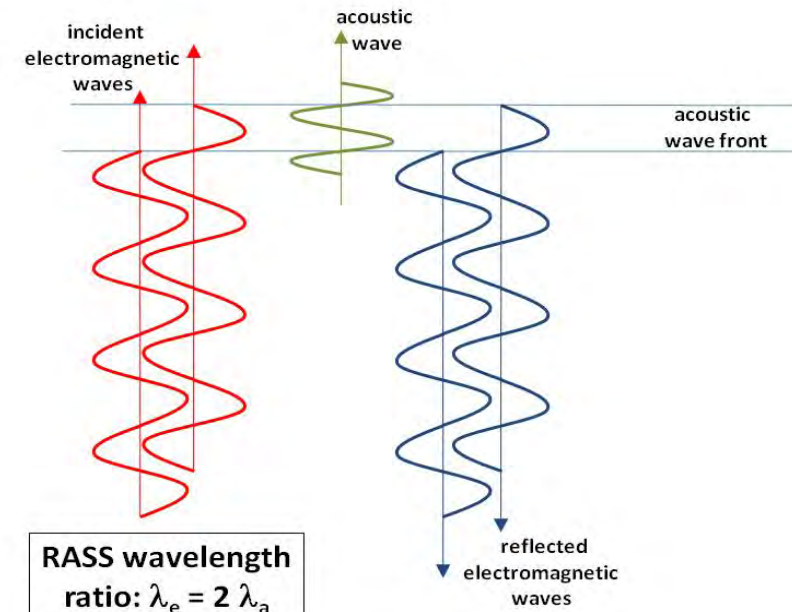
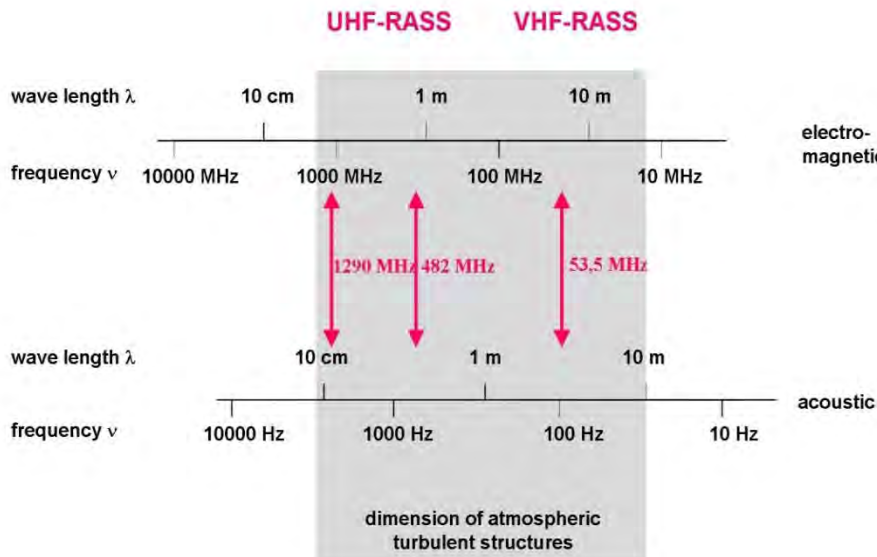
detection:

travel time of em./ac. signal	= height	
ac. backscatter intensity	= turbulence	(identical to SODAR)
ac. Doppler-shift	= line-of-sight wind speed	(identical to SODAR)
em. Doppler shift	= sound speed → temperature	

RASS: frequencies

Bragg condition:
acoustic wavelength = $\frac{1}{2}$ electro-magnetic wavelength

electro-magnetic - acoustic frequency pairs for RASS devices



Emeis, S., 2010: Measurement Methods in Atmospheric Sciences - In situ and remote. Borntraeger, Stuttgart, 272 pp., 103 figs, 28 tables, ISBN 978-3-443-01066-9.



SODAR-RASS (Doppler-RASS) (METEK)

acoustic frequ.: 1077 Hz

radio frequ.: 474 MHz

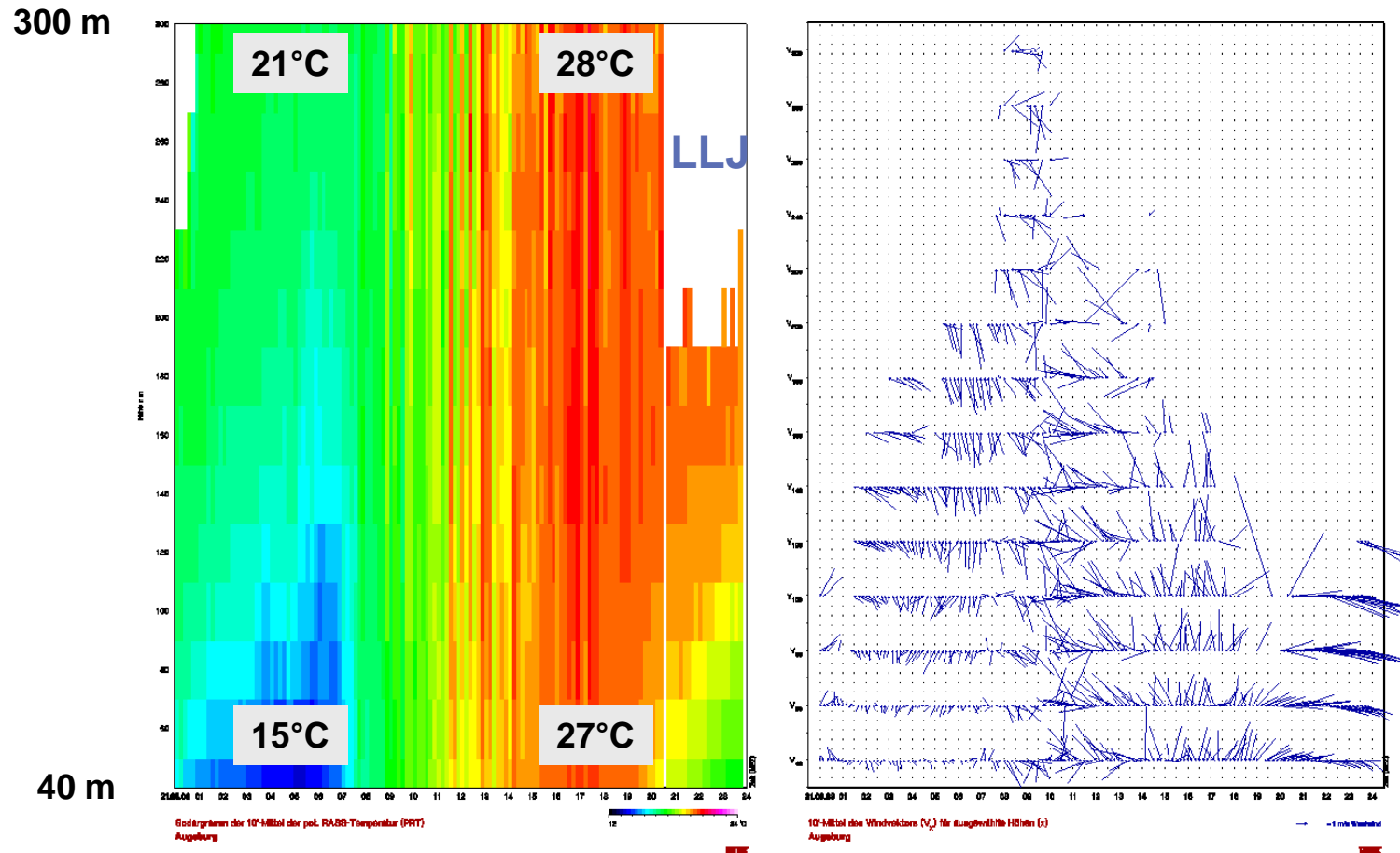
resolution: 20 m

lowest

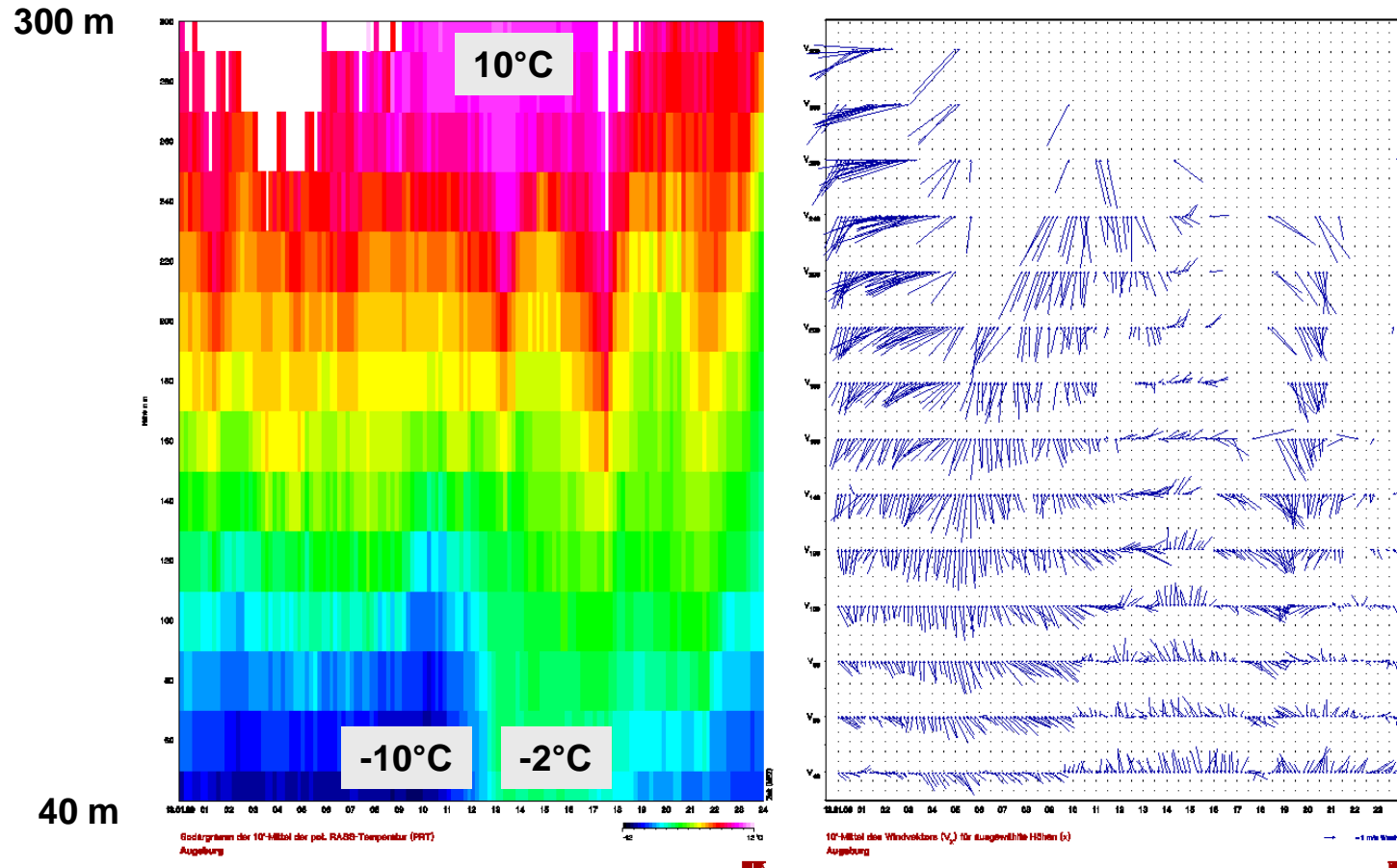
range gate: ca. 40 m

vertical range: 540 m

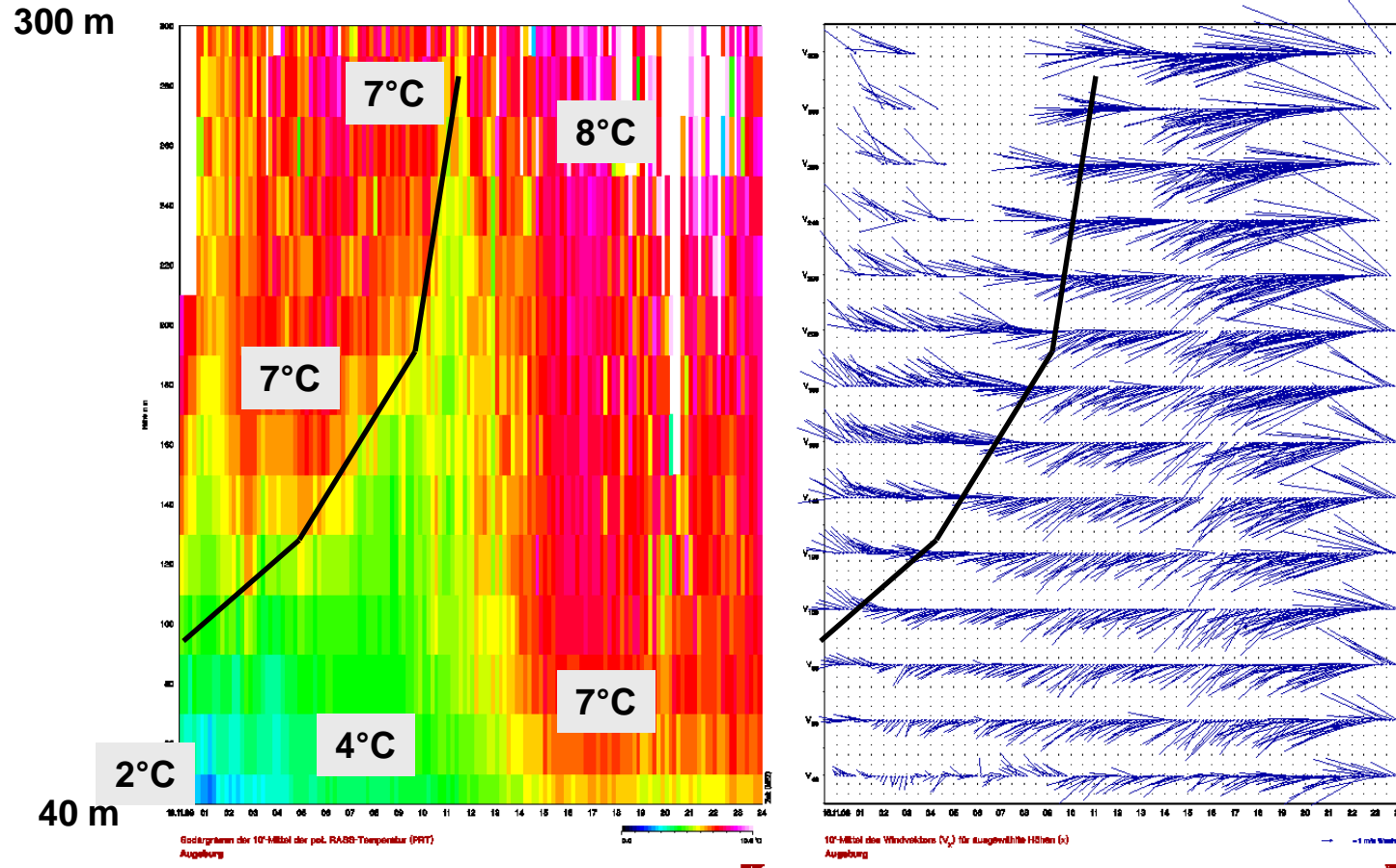
example RASS data: summer day potential temperature (left), horizontal wind (right)



example RASS data: winter day potential temperature (left), horizontal wind (right)



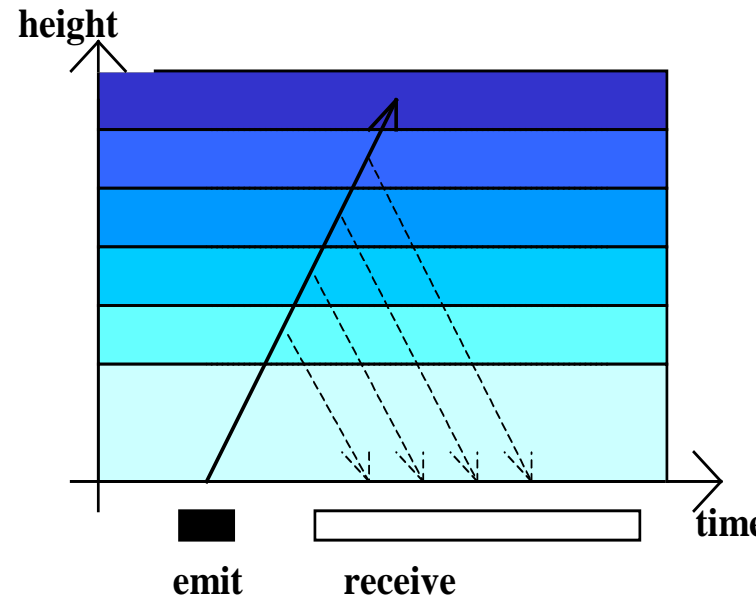
example RASS data: inversion potential temperature (left), horizontal wind (right)



Doppler windlidar

**wind, turbulence, aerosol detection,
mixing-layer height, low-level jet**

Doppler windlidar measuring principle

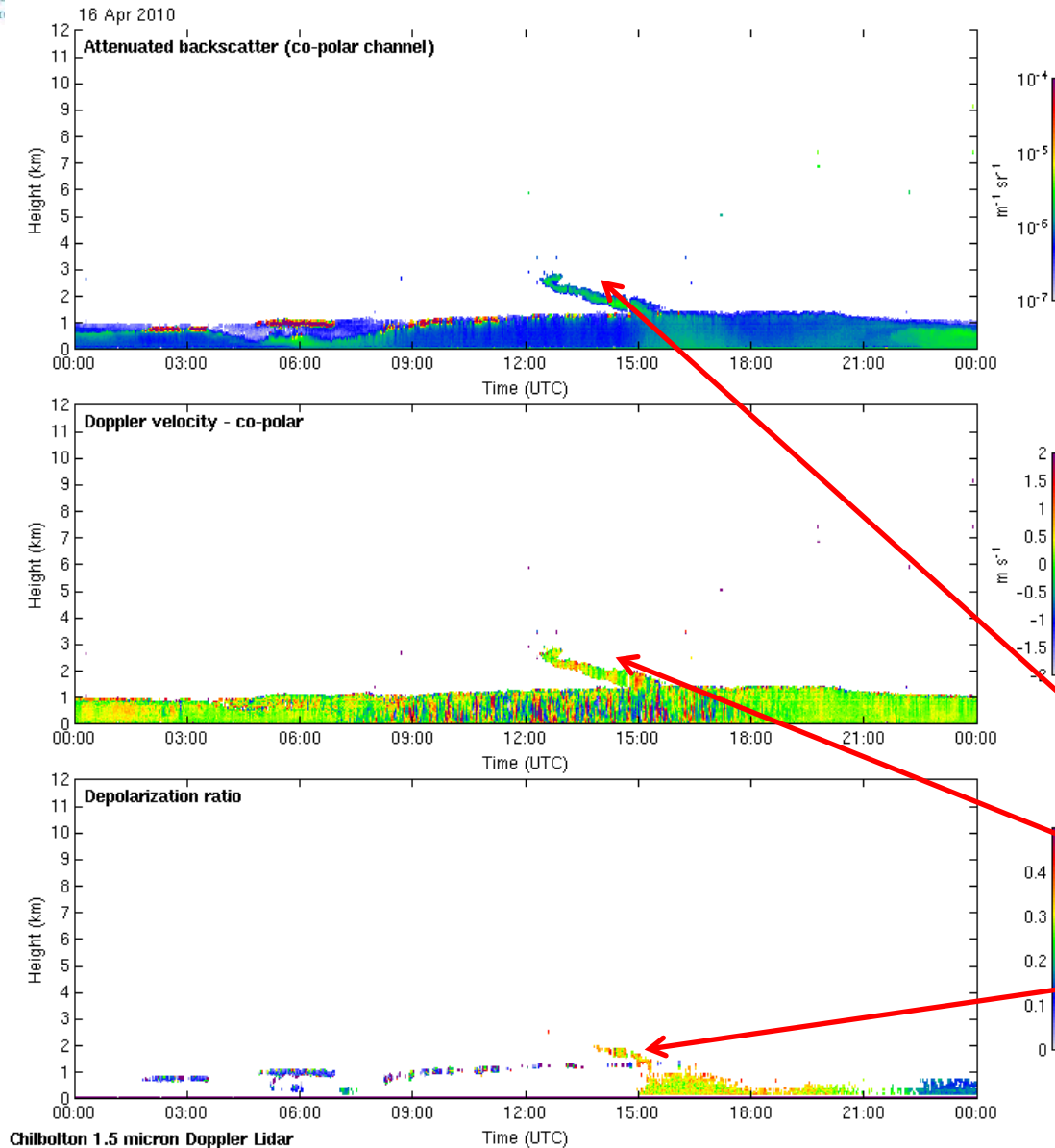


detection:

travel time of signal	= height
backscatter intensity	= particle size and number distribution
depolarisation	= particle shape
Doppler-shift	= wind speed in the line of sight

mobile Doppler windlidar from Halo Photonics





sample data from
windlidar

April 16, 2010

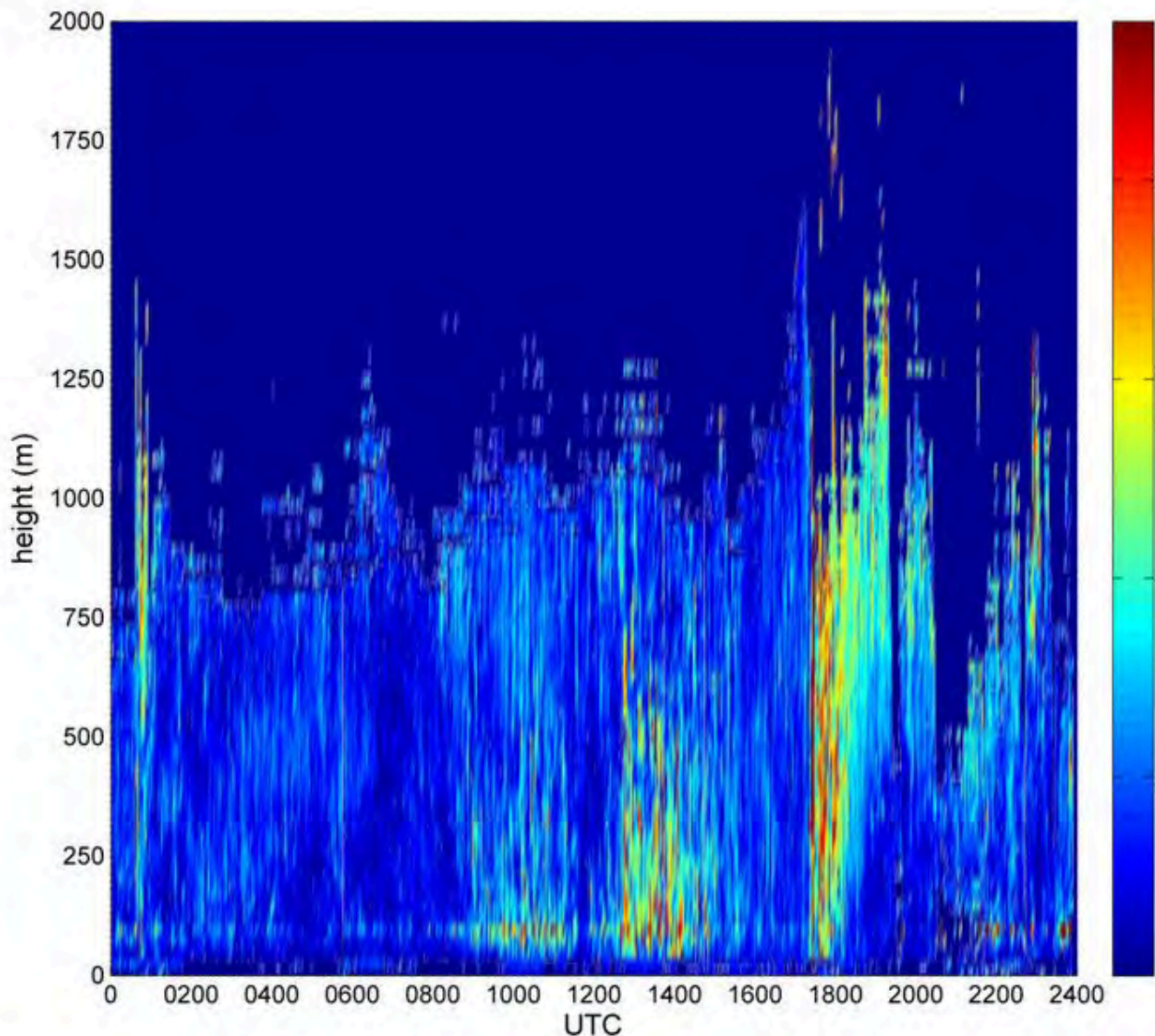
by
Univ. of Reading

taken at

Chilbolton, UK

[http://www.met.reading.ac.uk/
radar/realtime/archive/doppler-lidar/
20100416_chilbolton_halo-doppler-lidar.png](http://www.met.reading.ac.uk/radar/realtime/archive/doppler-lidar/20100416_chilbolton_halo-doppler-lidar.png)

volcanic ash
from
Eyjafjallajokull



**sample data from
windlidar**

**wind speeds in m/s
(colour bar)**

June 22, 2011

by IMK-IFU

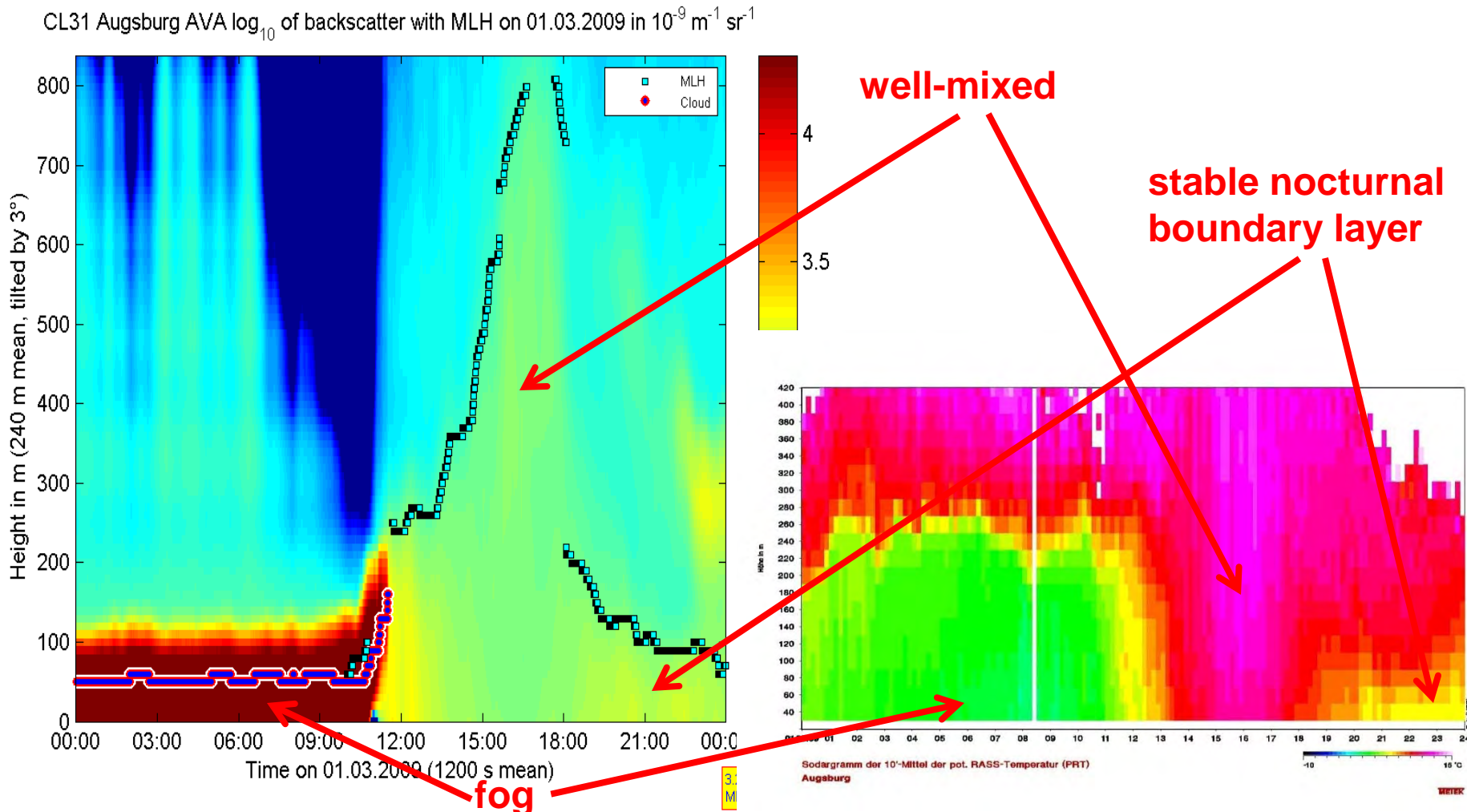
taken at

**Garmisch-Partenkirchen,
Germany**

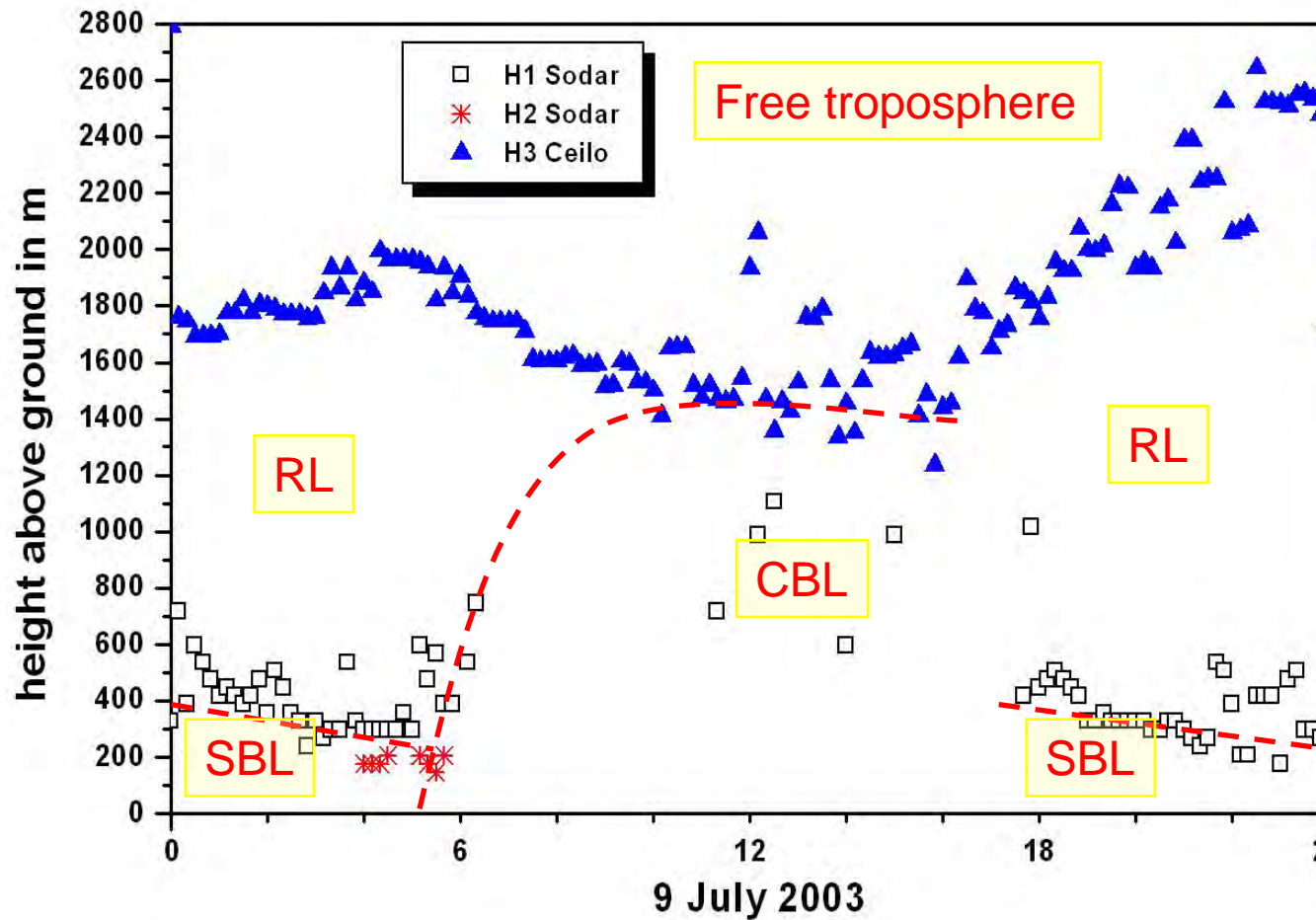
Comparisons between different instruments

temperature profile and aerosol backscatter

comparison of RASS data (potential temperature, right)
with aerosol backscatter from a ceilometer (left)

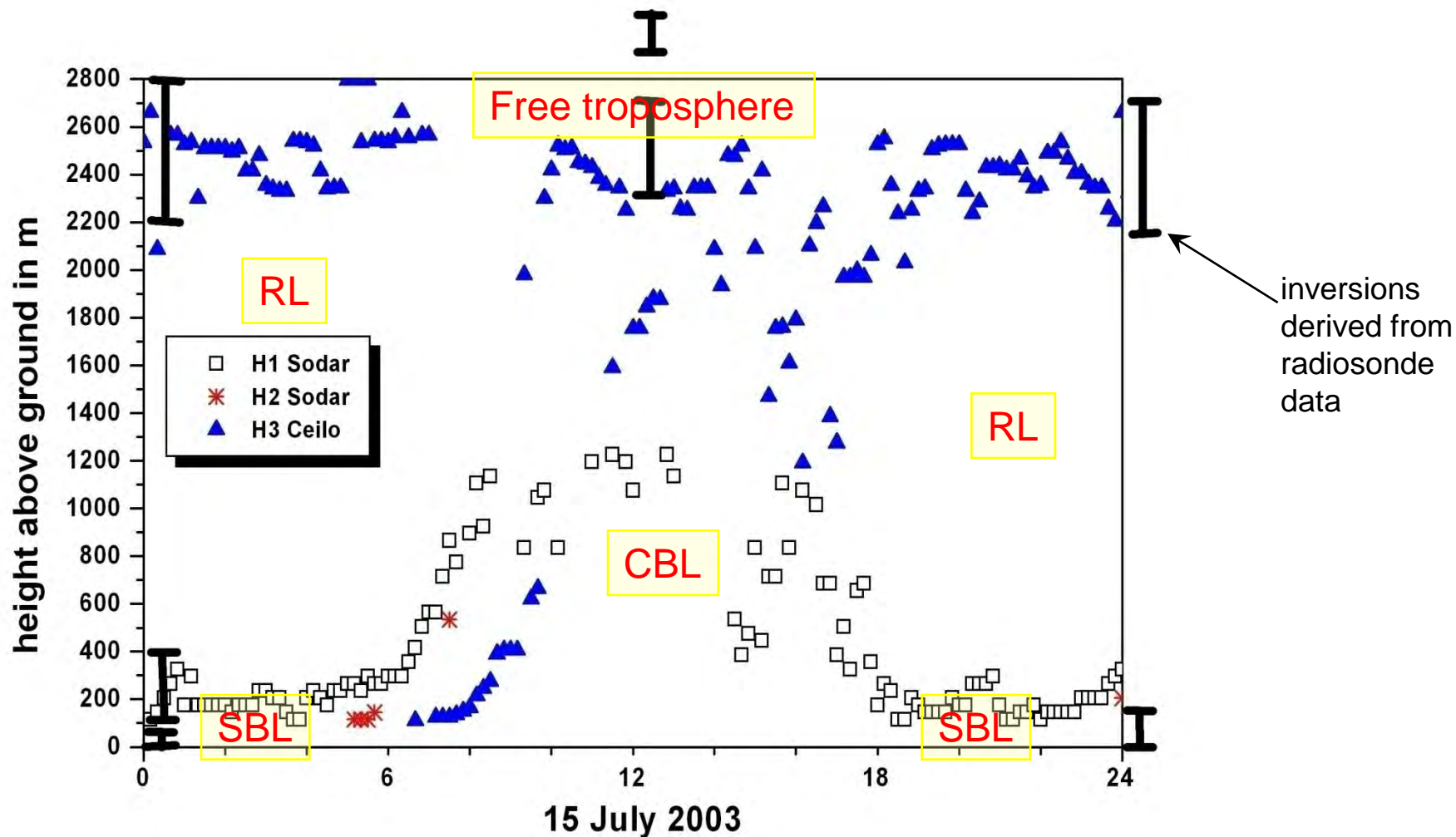


Detection of the diurnal variation of PBL structure from SODAR and Ceilometer data taken in Budapest



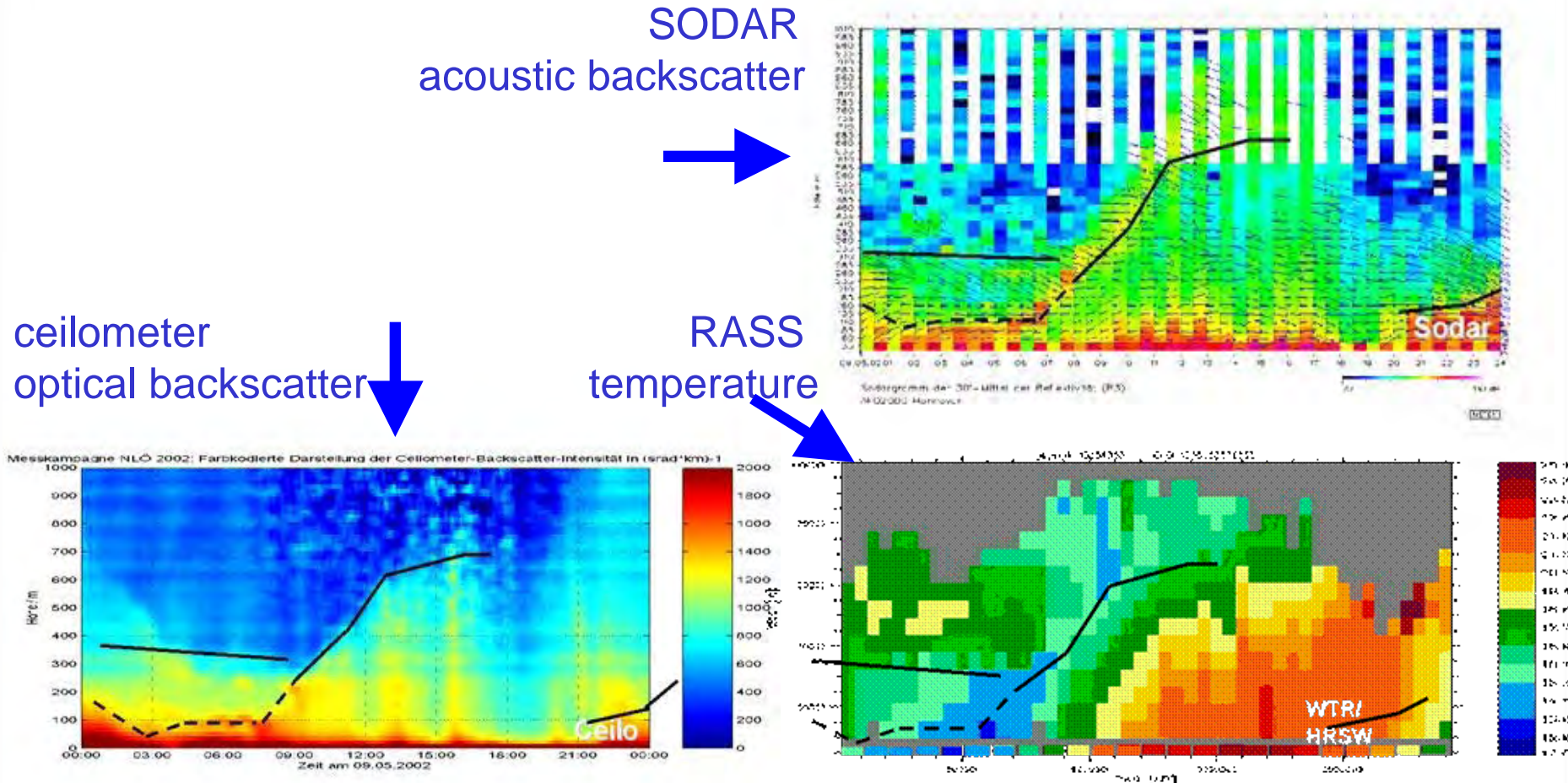
Emeis, S., K. Schäfer, 2006: Remote sensing methods to investigate boundary-layer structures relevant to air pollution in cities. Bound.-Lay Meteorol., 121, 377-385,

Differences in MLH detection from SODAR and Ceilometer data taken in Budapest



Emeis, S., K. Schäfer, 2006: Remote sensing methods to investigate boundary-layer structures relevant to air pollution in cities. Bound.-Lay Meteorol., 121, 377-385,

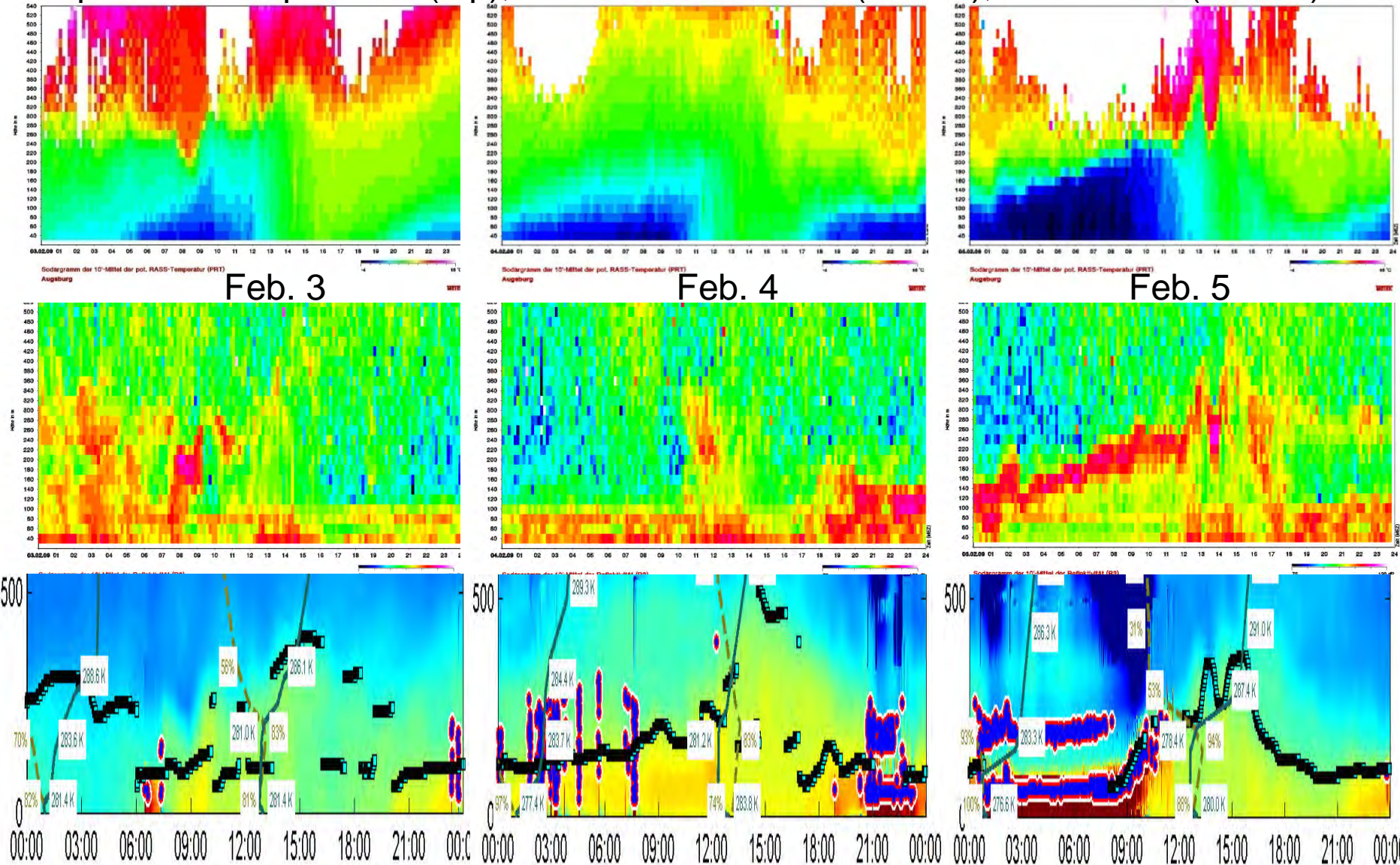
Comparison of MLH retrievals with three different remote sensing techniques



Emeis, S., Chr. Münkel, S. Vogt, W.J. Müller, K. Schäfer, 2004: Atmospheric boundary-layer structure from simultaneous SODAR, RASS, and ceilometer measurements. *Atmos. Environ.*, 38, 273-286.

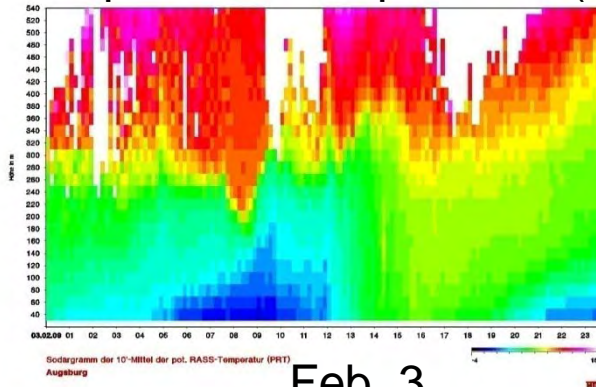
RASS data Augsburg February 2009

potential temperature (top), backscatter SODAR (middle), Ceilometer (bottom)

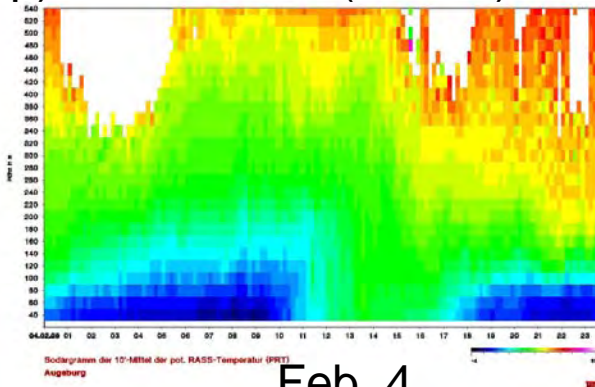


RASS data Augsburg February 2009

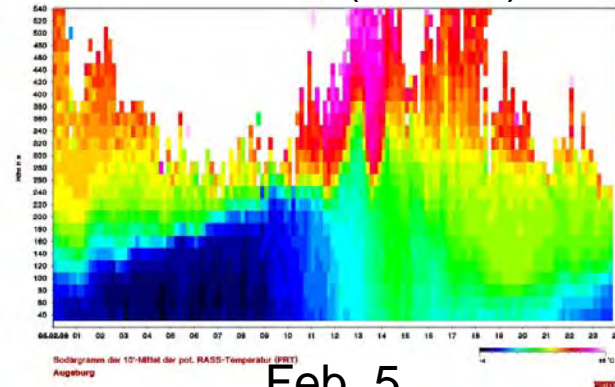
potential temperature (top), MLH RASS (middle), MHL SODAR/Ceilo (bottom)



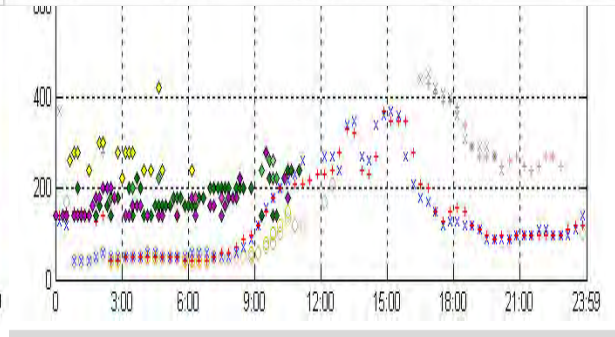
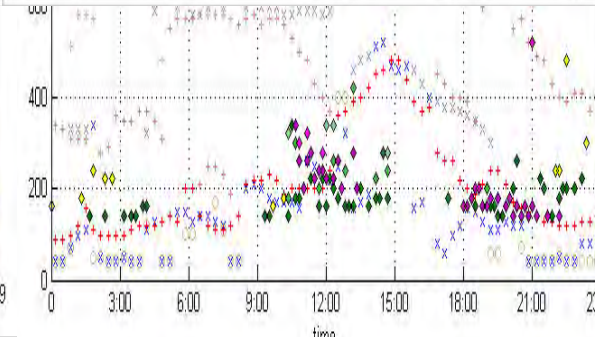
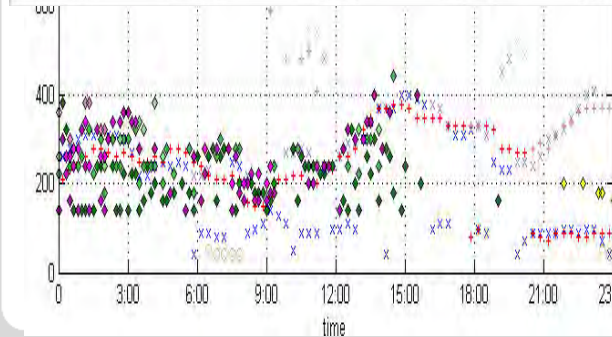
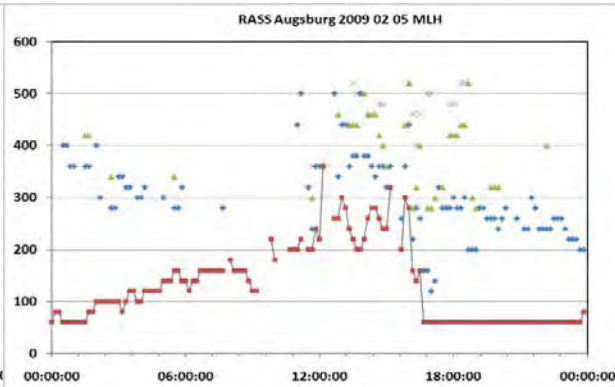
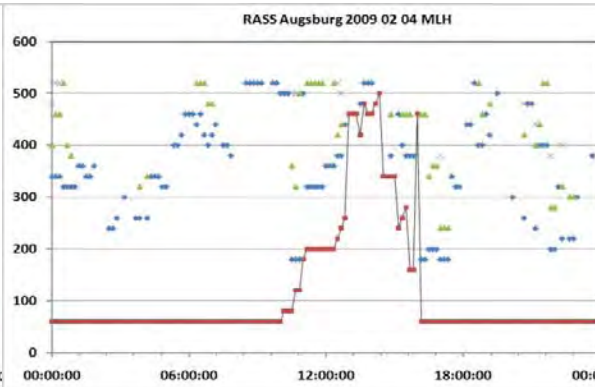
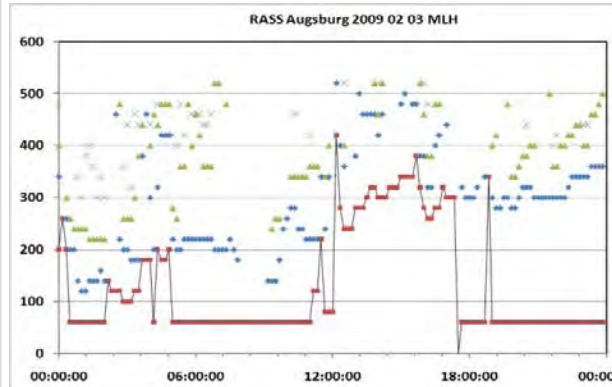
Feb. 3



Feb. 4



Feb. 5



Application of MLH information for regional emission flux estimates

Determination of regional surface emission fluxes of a substance e

Assumptions:

- horizontal homogeneity
- no fluxes through the upper boundary (inversion)
- no sources and sinks within the volume of interest

$$\int_{S_{surf}} \overline{e'w'} \cdot dS = \int_V \frac{de}{dt} dV$$

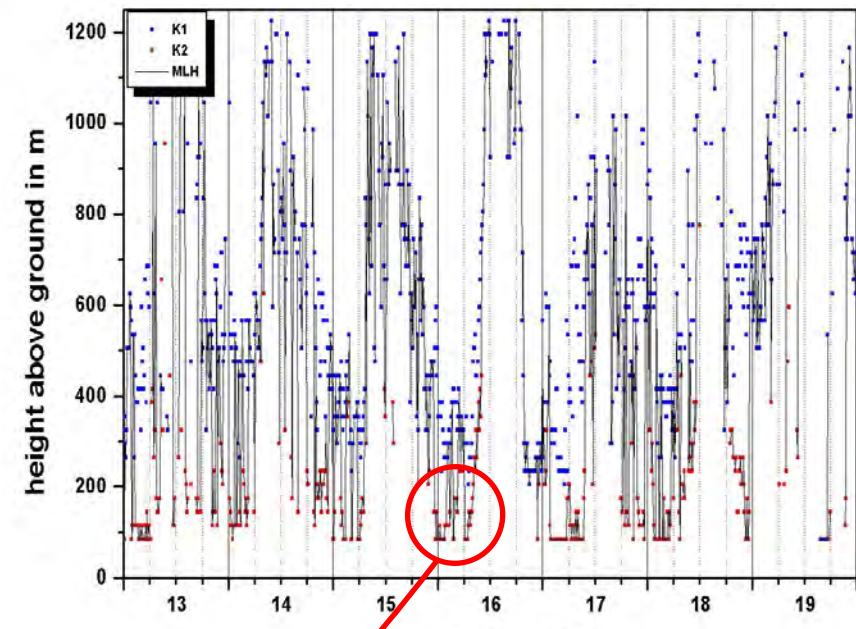
simultaneous measurement of concentration and MLH

(inverse method)

C_{CH_4}



MLH



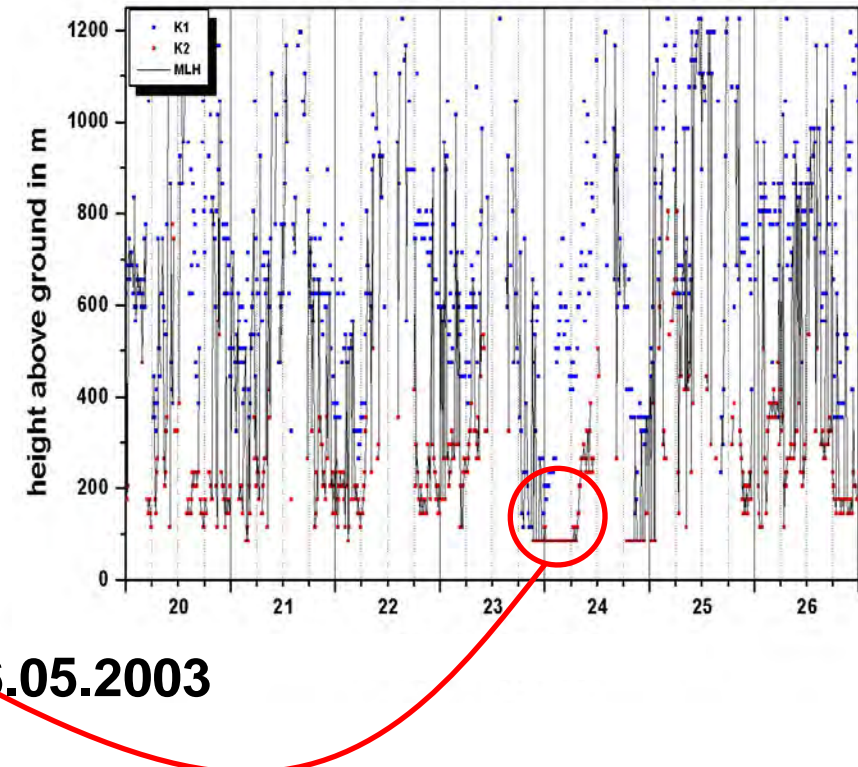
simultaneous measurement of concentration and MLH

(inverse method)

C_{CH_4}

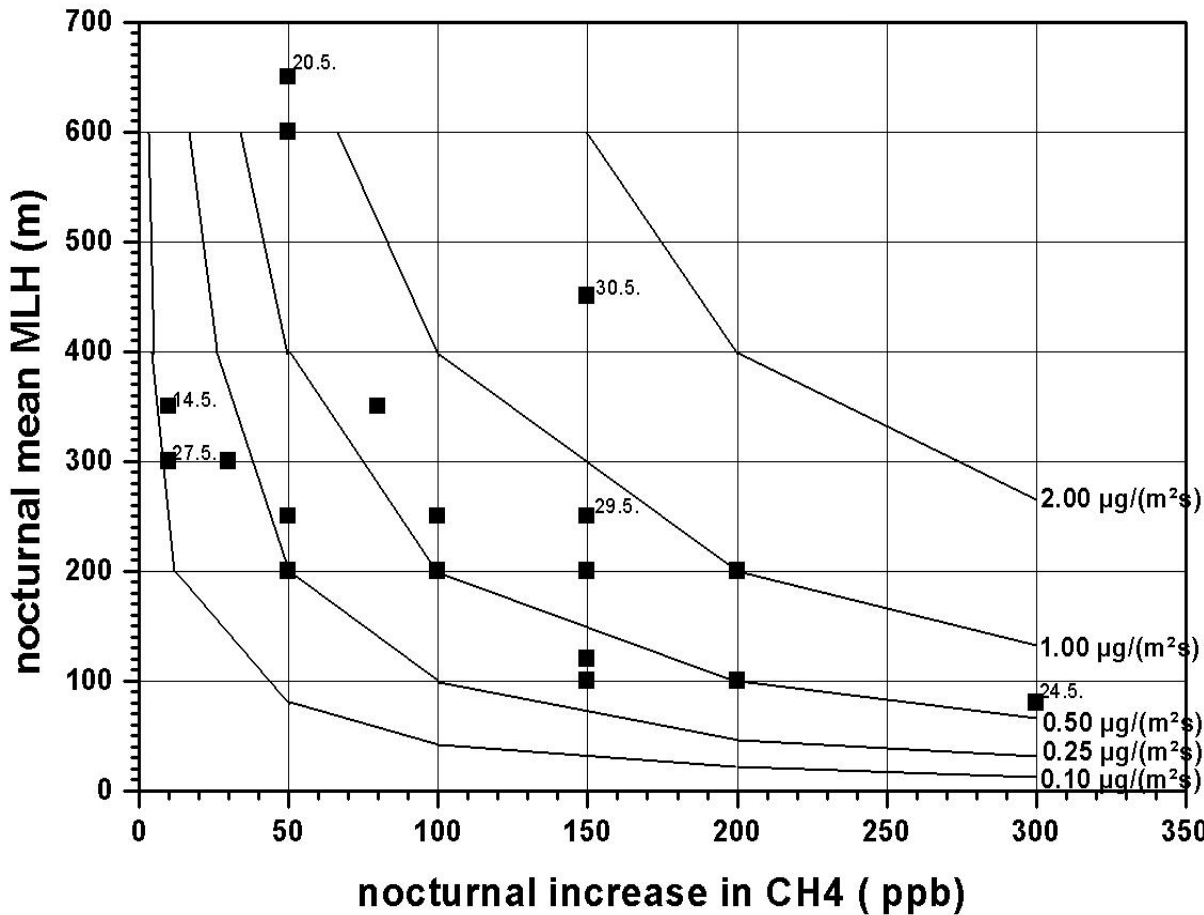


MLH



20.-26.05.2003

determination of regional $[C_{CH_4}^{'w}]_{surf}$ (curves) from concentration changes (x-axis) and MLH (y-axis)



determination of regional $[C_{CH_4}^{'w}]_{surf}$ (curves) from concentration changes and remotely sensed MLH

methane emissions:

typical values obtained here:

span:	0.10 to 2.00 $\mu\text{g}/(\text{m}^2 \text{s})$
mean value:	0.50 $\mu\text{g}/(\text{m}^2 \text{s})$

average values from national reporting (Kyoto protocol):

for entire Germany:	0.20 $\mu\text{g}/(\text{m}^2 \text{s})$
among this from agriculture:	0.13 $\mu\text{g}/(\text{m}^2 \text{s})$

Summary

😊 😊 😊 💯 **RASS** delivers temperature profiles, wind profiles are additionally available.
MLH directly from temperature profiles. LLJ from wind profiles.
Does not work properly under high wind speeds. Restricted range.

😊 😊 😊 💯 **wind lidar** detects wind profiles, aerosol distribution and water droplets.
It has to be assumed that the aerosol follows the thermal structure of the atmosphere and the wind.
MLH from aerosol backscatter, wind speed variance, LLJ from wind profiles.
Does not work properly in extreme clear (aerosol-free) air and during precipitation events and fog.

😊 😊 💯 💯 **Ceilometer** detects aerosol distribution and water droplets. It has to be assumed that the aerosol follows the thermal structure of the atmosphere.
MLH indirectly from aerosol backscatter using a MLH algorithm.
Does not work properly in extreme clear (aerosol-free) air and during precipitation events and fog.

😊 💯 💯 💯 💯 **SODAR** detects wind profiles, temperature fluctuations and gradients, but no absolute temperature.
MLH indirectly from acoustic backscatter (MLH algorithm). LLJ from wind profiles.
Does not work properly under perfectly neutral stratification, with very high wind speeds, and during stronger precipitation events. Restricted range.

Literature

Asimakopoulos, D.N., C.G. Helmis, J. Michopoulos, 2004: Evaluation of SODAR methods for the determination of the atmospheric boundary layer mixing height. - Meteor. Atmos. Phys. 85, 85–92.

Beyrich, F., 1997: Mixing height estimation from sodar data – a critical discussion. - Atmos. Environ. 31, 3941–3953.

Ceilometer:

Schäfer, K., S.M. Emeis, A. Rauch, C. Münkel, S. Vogt, 2004: Determination of mixing-layer heights from ceilometer data. In: Remote Sensing of Clouds and the Atmosphere IX. Schäfer, K., A. Comeron, M. Carleer, R.H. Picard, N. Sifakis (Eds.), Proc. SPIE, Bellingham, WA, USA, Vol. 5571, 248–259.

Sicard, M., C. Pérez, F. Rocadenbosch, J.M. Baldasano, D. García-Vizcaino, 2006: Mixed-Layer Depth Determination in the Barcelona Coastal Area From Regular Lidar Measurements: Methods, Results and Limitations. - Bound.-Lay. Meteor. 119, 135–157.

RASS:

Engelbart, D.A.M., J. Bange, 2002: Determination of boundary-layer parameters using wind profiler/RASS and sodar/RASS in the frame of the LITFASS project. Theor. Appl. Climatol. 73, 53–65.

Emeis, S., K. Schäfer, C. Münkel, 2009: Observation of the structure of the urban boundary layer with different ceilometers and validation by RASS data. Meteorol. Z., 18, 149-154. ([Open access, freely available from
http://dx.doi.org/10.1127/0941-2948/2009/0365](http://dx.doi.org/10.1127/0941-2948/2009/0365))

Emeis, S., K. Schäfer, C. Münkel, R. Friedl, P. Suppan, 2011: Evaluation of the interpretation of ceilometer data with RASS and radiosonde data. Bound.-Lay. Meteorol., online April 5, 2011. DOI: [10.1007/s10546-011-9604-6](https://doi.org/10.1007/s10546-011-9604-6)

Windlidar:

Emeis, S., M. Harris, R.M. Banta, 2007: Boundary-layer anemometry by optical remote sensing for wind energy applications. - Meteorol. Z., 16, 337-347.

Regional budget studies:

Emeis, S., 2008: Examples for the determination of turbulent (sub-synoptic) fluxes with inverse methods. Meteorol. Z., 17, 3-11. DOI: 10.1127/0941-2948/2008/0265

Reviews:

Emeis, S., K. Schäfer, C. Münkel, 2008: Surface-based remote sensing of the mixing-layer height – a review. - Meteorol. Z., 17, 621-630. (Open access, freely available from <http://dx.doi.org/10.1127/0941-2948/2008/0312>)

Books:

boundary-layer remote sensing with application examples:

Emeis, S., 2011: Surface-Based Remote Sensing of the Atmospheric Boundary Layer. Series: Atmospheric and Oceanographic Sciences Library, Vol. 40. Springer Heidelberg etc., X+174 pp. 114 illus., 57 in color., H/C. ISBN: 978-90-481-9339-4, DOI: 10.1007/978-90-481-9340-0

overview on the entire range of meteorological measurement methods:

Emeis, S., 2010: Measurement Methods in Atmospheric Sciences. In situ and remote. Series: Quantifying the Environment Vol. 1. Borntraeger Stuttgart. XIV+257 pp., 103 Figs, 28 Tab. ISBN 978-3-443-01066-9.

Thank you very
much for your
attention